Table 3
Echocardiographic measurements in TAC-APA5 or TAC-IgG mice

	TAC-IgG	TAC-APA5
Number	10	10
HW/BW (mg/g)	5.71 ± 0.18	5.67 ± 0.16
HR (bpm)	633.30 ± 16.06	657.00 ± 11.91
LVDd (mm)	3.54 ± 0.09	3.59 ± 0.08
LVDs (mm)	2.07 ± 0.09	2.01 ± 0.09
FS (%)	41.7 ± 1.48	44.2 ± 1.51
LVPWth (mm)	0.84 ± 0.01	0.81 ± 0.01

Mast cell stabilization and BM reconstitution. For stabilization of mast cells, cromolyn (50 mg/kg/day; Sigma-Aldrich) or vehicle was administrated daily to mice by i.p. injection (14) for the duration of the experiment (10 days after TAC operation). For BM reconstitution, BM cell suspensions were harvested by flushing the femurs and tibias of 8-week-old W/W^v or +/+ mice. The 5-week-old C57BL/6 mice were preconditioned with total body irradiation (9.5 Gy) 6 hours before transplantation. BM cell suspensions (1.0×10^7 cells per mouse) were transfused via the tail vein to the preconditioned recipient mice. The recipient mice were subjected to BM reconstitution for 6 weeks and were subjected to TAC operation.

Induction of AF in ex vivo and in vivo hearts. For induction of AF in ex vivo hearts, hearts were rapidly excised after i.p. injection of heparin (0.5 U/g) and urethane (2 mg/g) and immediately mounted onto a Langendorff perfusion apparatus (42). The hearts were perfused with a nonrecirculating Krebs-Henseleit buffer (119 mM NaCl, 4.8 mM KCl, 1.2 mM KH_2PO_4, 1.2 mM $MgSO_4$, 2.5 mM $CaCl_2$, 10 mM glucose, and 24.9 mM $NaHCO_3$), which was equilibrated with 5% CO_2/95% O_2 at 37°C. All isolated hearts were stabilized for 5 minutes by perfusion at constant flow (3.0 ± 0.2 ml/min) before programmed electrical stimulation. The whole system temperature was kept at 37°C. Two chlorinated silver wires were placed on the base of the heart as indifferent and common ground electrodes. A pair of recording electrodes were placed on the apex and anterior wall of the heart to record ventricular electrograms. Bipolar stimulating electrodes were pressed against the right atrium surface, and bipolar recording electrodes were placed on the left atrium surface to record atrial electrograms.

For induction of AF in in vivo hearts, mice were anesthetized with i.p. injection of pentobarbital and supported by artificial ventilation. The body temperature of mice was monitored and kept at 37°C using a heating pad during the experiments. A 2-French catheter electrode (Japan Lifeline) was placed at the esophageal position dorsal to the left atrium. A surface ECG was simultaneously recorded using electrodes in a lead-II configuration.

Inducibility of AF was tested by applying a 2-second burst using the automated stimulator. The first 2-second burst had a cycle length (CL) of 40 ms, decreasing in each successive burst with a 2-microsecond decrement down to a CL of 20 ms. A series of bursts was repeated 3 times after stabilization for 5 minutes. AF duration was defined as the interval between the rapid irregular atrial rhythm triggered after the bursts and the onset of first normal sinus beat.

Histological analysis. Hearts were excised and immediately fixed in 10% neutralized formalin, and they were then embedded in paraffin. Serial sections of atrium at 5 μm were stained with Masson's trichrome for evaluation of fibrosis. We determined mast cell number and morphology with toluidine blue staining (0.1%; Sigma-Aldrich) and rhodamine-avidin staining (1:100; Vector Laboratories) (20, 26). Specificity of mast cell detection was confirmed by staining sections of W/W^v and +/+ mice at the same dilution of the reagent. The total number of mast cells was counted manually and blindly in 3 microscopic sections from each mouse, and the total area was determined using computer-assisted image analysis (ImageJ; http://rsbweb.nih.gov/ij/).

Hydroxyproline assay. We evaluated collagen content in the atrium by quantification of hydroxyproline, as described previously (43). In brief, the atrium was weighed and then hydrolyzed in 6 N HCl at 100°C overnight. Hydrolyzed tissue was neutralized with NaOH, vacuum dried at 50°C, and resuspended in 1 ml of 5 mM HCl. An aliquot of 20 μl hydrolyzed tissue was added to 180 μl of H_2O in a glass tube. Thereafter, we mixed 100 μl of chloramine-T solution (0.14 g chloramine-T, Sigma-Aldrich; 2 ml H_2O, 8 ml hydroxyproline assay buffer) with the diluted hydrolyzed tissue solution. The ingredients of hydroxyproline assay buffer were as follows: 11.4 g sodium acetate anhydrous (Sigma-Aldrich), 7.5 g trisodium citrate dihydrate (Sigma-Aldrich), 40 ml H_2O (pH adjusted to 6.0), and 77 ml isopropanol, bringing the final volume to 200 ml with H_2O. After incubation for 10 minutes at room temperature, 1.25 ml Ehrlich's reagent (6.0 g p-dimethylaminobenzaldehyde [Sigma-Aldrich], 18 ml 60% perchlorate [Fluka], 78 ml isopropanol) was added and mixed. The samples were incubated at 55°C for 20–25 minutes, and the sample absorbance was read at 558 nm. We used *trans*-4-hydroxy-L-proline (Sigma-Aldrich) (ranging from 0 to 4 mg) to draw the standard curve.

Coculture of BMMCs with cardiac myocytes or fibroblasts. The BM cells were harvested from C57BL/6 mice and cultured for 5 weeks in RPMI 1640 medium (GIBCO; Invitrogen) supplemented with 10% FBS (Equitech-Bio), 0.1 mM MEM Non-Essential Amino Acids Solution (GIBCO; Invitrogen), 4 mM L-glutamine, 25 mM HEPES, 1 mM sodium pyruvate, 50 μM β-mercaptoethanol, 100 U/ml penicillin, 100 μg/ml streptomycin, and 30 ng/ml of recombinant murine IL-3 (PeproTech GmbH) at 37°C in 5% CO_2 (44). By 5 weeks in culture, mast cells were enriched to more than 95%, as assessed by the presence of metachromatic granules in toluidine blue–stained cells and by cell-surface expression of FcεRI (Upstate) using flow cytometric analysis. The cardiac myocytes and fibroblasts were prepared from hearts of 1-day-old Wistar rats, as described previously (45). Dissociated cells were preplated onto 10-cm culture dishes for 30 minutes, which permitted preferential attachment of fibroblasts to the bottom of the dish. Nonadherent cardiac myocytes (3.5×10^5 cells/3.5-cm dish) or adherent fibroblasts (2.0×10^6 cells/3.5-cm dish) were plated on 3.5-cm dishes and cultured for 24 hours in medium (DMEM [GIBCO; Invitrogen], supplemented with 10% FBS, 100 U/ml penicillin, and 100 μg/ml streptomycin). The cells were starved under a serum-free condition for 24 hours before initiation of the coculture. BMMCs (5.0×10^6 cells/3.5-cm dish) were placed onto layers of cardiac myocytes or fibroblasts and were continuously cocultured in DMEM without supplementation with FBS. For stabilization of BMMCs in vitro, BMMCs were pretreated with 10^{-5} M cromolyn (Sigma-Aldrich) for 30 minutes before initiation of coculture, and cromolyn treatment was continued throughout the coculture.

Real-time RT-PCR analysis. Total RNA was extracted by using RNeasy Kit (QIAGEN), and single-stranded cDNA was transcribed by using QuantiTect Reverse Transcription Kit (QIAGEN) according to the manufacturer's protocol. We conducted quantitative real-time PCR analysis with the Universal ProbeLibrary Assays (Roche Applied Science) according to the manufacturer's instructions. Amplification conditions were as follows: initial denaturation for 10 minutes at 95°C followed by 45 cycles of 10 seconds at 95°C and 25 seconds at 60°C. Individual PCR products were analyzed by melting-point analysis. The expression level of a gene was normalized relative to that of *Gapdh* by using a comparative Ct method. The primer sequences and universal probe numbers were designed with the ProbeFinder software as follows: *Pdgfa*, 5′-GTGCGACCTCCAACCTGA-3′ and 5′-GGCTCATCTCACCTCACATCT-3′, no. 52; *Pdgfb*, 5′-CGGCCTGTGACTAGAAGTCC-3′ and 5′-GAGCTTGAGGCGTCTTGG-3′, no. 32; *Col3a1*, 5′-TCCCCTG-

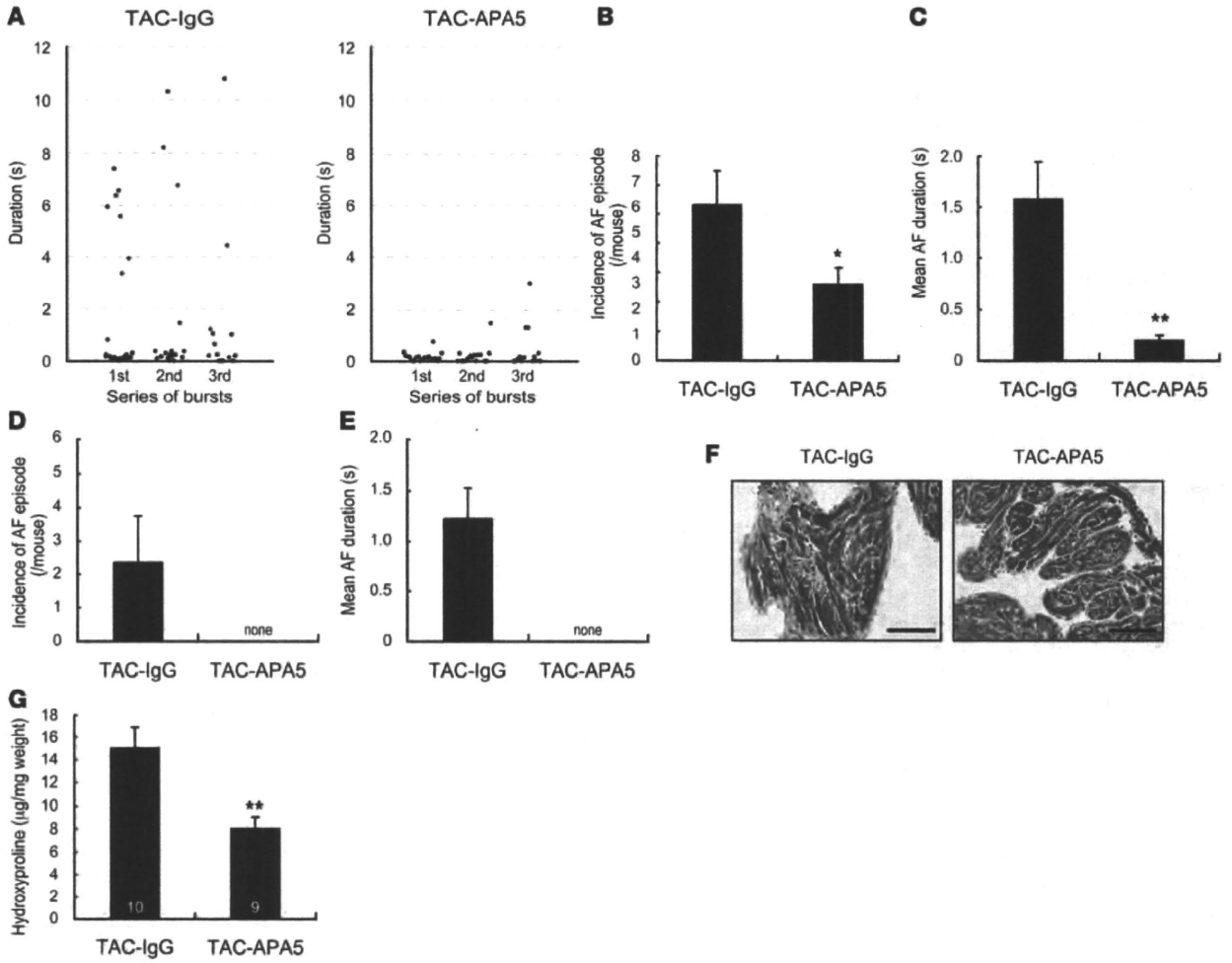

Figure 8

Attenuation of atrial fibrosis and AF by neutralization of PDGFR-α. (**A**) Scatter plot of duration of AF episodes occurring during 3 series of bursts under Langendorff perfusion in TAC-APA5 ($n = 9$) or TAC-IgG mice ($n = 9$). (**B**) Incidence of AF episodes during 3 series of bursts under Langendorff perfusion ($n = 9$). $^{*}P < 0.05$ versus control IgG. (**C**) Mean duration of AF episodes during 3 series of bursts under Langendorff perfusion ($n = 9$). $^{**}P < 0.01$ versus control IgG. (**D**) Incidence of AF episodes during 3 series of transesophageal bursts ($n = 6$). (**E**) Mean duration of AF episodes during 3 series of transesophageal bursts ($n = 6$). (**F**) Representative histological sections with Masson's trichrome staining for visualization of atrial fibrosis (blue staining). Scale bars: 20 μm. (**G**) Hydroxyproline content in the atrium ($n = 9$). Number of mice for each experiment is indicated in the bars. $^{**}P < 0.01$ versus control IgG. Data are presented as mean ± SEM.

GAATCTGTGAATC-3′ and 5′-TGAGTCGAATTGGGGAGAAT-3′, no. 49; mouse *Gapdh*, 5′-TGTCCGTCGTGGATCTGAC-3′ and 5′-CCTGCTTCAC-CACCTTCTTG-3′, no. 80; rat *Gapdh*, 5′-TGGGAAGCTGGTCATCAAC-3′ and 5′-GCATCACCCCATTTGATGTT-3′, no. 9.

ELISA of PDGF-AA. The concentrations of PDGF-AA in the conditioned medium were assayed by using Human/Mouse PDGF-AA Quantikine ELISA Kit (R&D Systems) according to the manufacturer's protocol.

Cell proliferation assay. Cardiac fibroblasts (2×10^4 cells/well) were plated on a 48-well plate and were cultured for 24 hours in medium (DMEM supplemented with 10% FBS, 100 U/ml penicillin, and 100 μg/ml streptomycin) at 37°C in 5% CO_2. After 24 hours of starvation under serum-free conditions, we replaced the medium with that conditioned by coculture of BMMCs and cardiac fibroblasts. After 24 hours of culture, cells were harvested, and subjected to semiquantification of the viable cell numbers that are proportional to the amount of ATP by using CellTiter-Glo Luminescent Cell Viability Assay Kit (Promega).

Systemic administration of PDGF-AA. Mini-osmotic pumps (model 2002; Alzet) were subcutaneously implanted in 10-week-old male mice to deliver recombinant murine PDGF-AA (0.2 μg/day; PeproTech) or vehicle. At 10 days after implantation, mice were sacrificed for analysis.

Inhibition of PDGF-A by a neutralizing anti–PDGFR-α antibody. To antagonize the effects of BMMC-derived PDGF-A in vitro, we pretreated BMMCs with 2 μg/ml of clone APA5 (200 μg/day) (27) or control IgG2a (eBioscience) for 30 minutes before initiation of coculture and continued the treatment throughout the coculture. To inhibit the effects of PDGF-A in vivo, we administered anti-PDGFR-α antibody (200 μg/day) (27) or control IgG2a by i.p. injection to mice for the duration of the experiment (10 days after TAC operation). APA5, a rat monoclonal anti-mouse PDGFR-α antibody (IgG2a), was described previously (46).

Statistics. All data are presented as means ± SEM. Two-group comparison was analyzed by unpaired 2-tailed Student's *t* test, and multiple-group comparison was performed by 1-way ANOVA followed by the Fisher's pro-

tected least significant difference test for comparison of means. $P < 0.05$ was considered to be statistically significant.

Acknowledgments

We are grateful to S. Nishikawa (Center for Developmental Biology, RIKEN, Japan) for providing APA5 hybridoma cells. We thank A. Furuyama, M. Ikeda, Y. Ohtsuki, I. Sakamoto, and M. Kikuchi for their excellent technical assistance. This work was supported in part by grants from the Japanese Ministry of Education, Science, Sports, and Culture, and Health and Labor Sciences Research grants (to I. Komuro and H. Akazawa); and grants from Japan Intractable Diseases Research Foundation and Takeda Science Foundation (to H. Akazawa).

Received for publication May 21, 2009, and accepted in revised form October 14, 2009.

Address correspondence to: Issei Komuro, Department of Cardiovascular Science and Medicine, Chiba University Graduate School of Medicine, 1-8-1 Inohana, Chuo-ku, Chiba 260-8670, Japan. Phone: 81-43-226-2097; Fax: 81-43-226-2557; E-mail: komuro-tky@umin.ac.jp.

1. Fuster V, et al. ACC/AHA/ESC 2006 guidelines for the management of patients with atrial fibrillation. *Circulation.* 2006;114(7):e257–354.
2. Nattel S. New ideas about atrial fibrillation 50 years on. *Nature.* 2002;415(6868):219–226.
3. Burstein B, Nattel S. Atrial fibrosis: mechanisms and clinical relevance in atrial fibrillation. *J Am Coll Cardiol.* 2008;51(8):802–809.
4. Corradi D, Callegari S, Maestri R, Benussi S, Alfieri O. Structural remodeling in atrial fibrillation. *Nat Clin Pract Cardiovasc Med.* 2008;5(12):782–796.
5. Frustaci A, et al. Histological substrate of atrial biopsies in patients with lone atrial fibrillation. *Circulation.* 1997;96(4):1180–1184.
6. Issac TT, Dokainish H, Lakkis NM. Role of inflammation in initiation and perpetuation of atrial fibrillation: a systematic review of the published data. *J Am Coll Cardiol.* 2007;50(21):2021–2028.
7. Nakamura Y, et al. Tissue factor expression in atrial endothelia associated with nonvalvular atrial fibrillation: possible involvement in intracardiac thrombogenesis. *Thromb Res.* 2003;111(3):137–142.
8. Verheule S, et al. Alterations in atrial electrophysiology and tissue structure in a canine model of chronic atrial dilatation due to mitral regurgitation. *Circulation.* 2003;107(20):2615–2622.
9. Chung MK, et al. C-reactive protein elevation in patients with atrial arrhythmias: inflammatory mechanisms and persistence of atrial fibrillation. *Circulation.* 2001;104(24):2886–2891.
10. Aviles RJ, et al. Inflammation as a risk factor for atrial fibrillation. *Circulation.* 2003;108(24):3006–3010.
11. Kalesnikoff J, Galli SJ. New developments in mast cell biology. *Nat Immunol.* 2008;9(11):1215–1223.
12. Metz M, Grimbaldeston MA, Nakae S, Piliponsky AM, Tsai M, Galli SJ. Mast cells in the promotion and limitation of chronic inflammation. *Immunol Rev.* 2007;217:304–328.
13. Sperr WR, et al. The human cardiac mast cell: localization, isolation, phenotype, and functional characterization. *Blood.* 1994;84(11):3876–3884.
14. Bot I, et al. Perivascular mast cells promote atherogenesis and induce plaque destabilization in apolipoprotein E-deficient mice. *Circulation.* 2007;115(19):2516–2525.
15. Sun J, et al. Mast cells promote atherosclerosis by releasing proinflammatory cytokines. *Nat Med.* 2007;13(6):719–724.
16. Sun J, et al. Mast cells modulate the pathogenesis of elastase-induced abdominal aortic aneurysms in mice. *J Clin Invest.* 2007;117(11):3359–3368.
17. Tsuruda T, et al. Adventitial mast cells contribute to pathogenesis in the progression of abdominal aortic aneurysm. *Circ Res.* 2008;102(11):1368–1377.
18. Hara M, et al. Evidence for a role of mast cells in the evolution to congestive heart failure. *J Exp Med.* 2002;195(3):375–381.
19. Higuchi H, et al. Mast cells play a critical role in the pathogenesis of viral myocarditis. *Circulation.* 2008;118(4):363–372.
20. Mackins CJ, et al. Cardiac mast cell-derived renin promotes local angiotensin formation, norepinephrine release, and arrhythmias in ischemia/reperfusion. *J Clin Invest.* 2006;116(4):1063–1070.
21. Cairns JA, Walls AF. Mast cell tryptase stimulates the synthesis of type I collagen in human lung fibroblasts. *J Clin Invest.* 1997;99(6):1313–1321.
22. Kondo S, et al. Role of mast cell tryptase in renal interstitial fibrosis. *J Am Soc Nephrol.* 2001;12(8):1668–1676.
23. Mori R, Shaw TJ, Martin P. Molecular mechanisms linking wound inflammation and fibrosis: knockdown of osteopontin leads to rapid repair and reduced scarring. *J Exp Med.* 2008;205(1):43–51.
24. Theoharides TC, Kempuraj D, Tagen M, Conti P, Kalogeromitros D. Differential release of mast cell mediators and the pathogenesis of inflammation. *Immunol Rev.* 2007;217:65–78.
25. Sano M, et al. p53-induced inhibition of Hif-1 causes cardiac dysfunction during pressure overload. *Nature.* 2007;446(7134):444–448.
26. Tharp MD, Seelig LL Jr, Tigelaar RE, Bergstresser PR. Conjugated avidin binds to mast cell granules. *J Histochem Cytochem.* 1985;33(1):27–32.
27. Zymek P, et al. The role of platelet-derived growth factor signaling in healing myocardial infarcts. *J Am Coll Cardiol.* 2006;48(11):2315–2323.
28. Olgin JE, Verheule S. Transgenic and knockout mouse models of atrial arrhythmias. *Cardiovasc Res.* 2002;54(2):280–286.
29. Kitamura Y, Go S, Hatanaka K. Decrease of mast cells in W/Wv mice and their increase by bone marrow transplantation. *Blood.* 1978;52(2):447–452.
30. Huizinga JD, et al. W/kit gene required for interstitial cells of Cajal and for intestinal pacemaker activity. *Nature.* 1995;373(6512):347–349.
31. Li M, et al. c-kit is required for cardiomyocyte terminal differentiation. *Circ Res.* 2008;102(6):677–685.
32. Lewis JP, O'Grady LF, Bernstein SE, Russell EE, Trobaugh FE, Jr. Growth and differentiation of transplanted W/Wv marrow. *Blood.* 1967;30(5):601–616.
33. Patella V, et al. Stem cell factor in mast cells and increased mast cell density in idiopathic and ischemic cardiomyopathy. *Circulation.* 1998;97(10):971–978.
34. Galli SJ, et al. Mast cells as "tunable" effector and immunoregulatory cells: recent advances. *Annu Rev Immunol.* 2005;23:749–786.
35. Thompson HL, Burbelo PD, Segui-Real B, Yamada Y, Metcalfe DD. Laminin promotes mast cell attachment. *J Immunol.* 1989;143(7):2323–2327.
36. Dastych J, Costa JJ, Thompson HL, Metcalfe DD. Mast cell adhesion to fibronectin. *Immunology.* 1991;73(4):478–484.
37. Bianchine PJ, Burd PR, Metcalfe DD. IL-3-dependent mast cells attach to plate-bound vitronectin. Demonstration of augmented proliferation in response to signals transduced via cell surface vitronectin receptors. *J Immunol.* 1992;149(11):3665–3671.
38. Bonner JC. Regulation of PDGF and its receptors in fibrotic diseases. *Cytokine Growth Factor Rev.* 2004;15(4):255–273.
39. Burstein B, Libby E, Calderone A, Nattel S. Differential behaviors of atrial versus ventricular fibroblasts: a potential role for platelet-derived growth factor in atrial-ventricular remodeling differences. *Circulation.* 2008;117(13):1630–1641.
40. Kumagai K, et al. Effects of angiotensin II type 1 receptor antagonist on electrical and structural remodeling in atrial fibrillation. *J Am Coll Cardiol.* 2003;41(12):2197–2204.
41. Nattel S, Shiroshita-Takeshita A, Brundel BJ, Rivard L. Mechanisms of atrial fibrillation: lessons from animal models. *Prog Cardiovasc Dis.* 2005;48(1):9–28.
42. Suzuki M, et al. Functional roles of cardiac and vascular ATP-sensitive potassium channels clarified by Kir6.2-knockout mice. *Circ Res.* 2001;88(6):570–577.
43. Oka T, et al. Cardiac-specific deletion of Gata4 reveals its requirement for hypertrophy, compensation, and myocyte viability. *Circ Res.* 2006;98(6):837–845.
44. Jensen BM, Swindle EJ, Iwai S, Gilfillan AM. Generation, isolation, and maintenance of rodent mast cells and mast cell lines. In Coligan, JE, Bierer, B, Margulies, DH, Shevach, EM, Strober, W, Coico, R, eds. *Current Protocols in Immunology.* Hoboken, NJ: John Wiley & Sons; 2006:Chapter 3:Unit 3.23.
45. Zou Y, et al. Cell type-specific angiotensin II-evoked signal transduction pathways: critical roles of Gbetagamma subunit, Src family, and Ras in cardiac fibroblasts. *Circ Res.* 1998;82(3):337–345.
46. Takakura N, Yoshida H, Kunisada T, Nishikawa S, Nishikawa SI. Involvement of platelet-derived growth factor receptor-alpha in hair canal formation. *J Invest Dermatol.* 1996;107(5):770–777.

Inhibition of Semaphorin As a Novel Strategy for Therapeutic Angiogenesis

Junji Moriya,* Tohru Minamino,* Kaoru Tateno, Sho Okada, Akiyoshi Uemura, Ippei Shimizu, Masataka Yokoyama, Aika Nojima, Mitsuhiro Okada, Hisashi Koga, Issei Komuro

Rationale: The axon-guiding molecules known as semaphorins and their receptors (plexins) regulate the vascular pattern and play an important role in the development of vascular network during embryogenesis. Semaphorin (Sema)3E is one of the class 3 semaphorins, and plexinD1 is known to be its receptor. Although these molecules have a role in embryonic vascular development, it remains unclear whether the Sema3E/plexinD1 axis is involved in postnatal angiogenesis.

Objective: The objective of this study was to elucidate the role of Sema3E/plexinD1 in postnatal angiogenesis.

Methods and Results: Sema3E inhibited cell growth and tube formation by suppressing the vascular endothelial growth factor (VEGF) signaling pathway. Expression of Sema3E and plexinD1 was markedly upregulated in ischemic limbs of mice (2.5- and 4.5-fold increase for Sema3E and plexinD1, respectively), and inhibition of this pathway by introduction of the plexinD1-Fc gene or disruption of Sema3E led to a significant increase of blood flow recovery (1.6- and 1.5-fold increase for the plexinD1-Fc gene treatment and Sema3E disruption, respectively). Hypoxia activated the tumor suppressor protein p53, thereby upregulating Sema3E expression. Expression of p53 and Sema3E was enhanced in diabetic mice compared with normal mice (2- and 1.3-fold increase for p53 and Sema3E, respectively). Consequently, neovascularization after VEGF treatment was poor in the ischemic tissues of diabetic mice, whereas treatment with VEGF plus plexinD1-Fc markedly improved neovascularization.

Conclusions: These results indicate that inhibition of Sema3E may be a novel strategy for therapeutic angiogenesis, especially when VEGF is ineffective. (*Circ Res*. 2010;106:391-398.)

Key Words: angiogenesis ■ semaphorins ■ p53 ■ diabetes

The vascular system and nervous system have several striking anatomic similarities. Recent findings have shown that the similarities between these systems extend to the molecular level and that the molecular mechanisms which are important for the specification, differentiation, and patterning of nerves also play an important role within the vasculature and vice versa.[1–4] Development of the nervous system is regulated through the coordinated action of a variety of repulsive or attractive neuronal guidance factors, called "axon-guiding molecules," that direct the growth of axons into specific pathways.[3] Recently, these axon-guiding molecules (including semaphorins) have also been shown to play a pivotal role in the formation of vascular networks.[1,5]

Semaphorins and their receptors (known as plexins) were initially characterized as signaling molecules that repel or attract axons,[6–9] but are now recognized as critical regulators of morphogenesis and homeostasis in various organs and systems.[10,11] The semaphorin family comprises 21 genes in vertebrates and eight additional genes are found in invertebrates. These genes are divided into eight classes on the basis of the similarity of their structural domains, with classes 3 to 7 containing the vertebrate semaphorins.[5] Class 3 are the only semaphorins secreted in vertebrates. Semaphorin (Sema)3E is one of the class 3 semaphorins,[12] and plexinD1 is known to be its receptor.[10] It has been reported that loss of plexinD1 or Sema3E causes abnormalities of vascular growth,[10] suggesting that these molecules have a crucial role in regulating the pattern of vessel development during embryogenesis.[13,14] However, it remains unknown whether Sema3E and plexinD1 are involved in postnatal angiogenesis.

Original received February 26, 2009; resubmission received October 7, 2009; revised resubmission received November 11, 2009; accepted November 13, 2009.

This manuscript was sent to Ingrid Fleming, Consulting Editor, for review by expert referees, editorial decision, and final disposition.

From the Department of Cardiovascular Science and Medicine (J.M., T.M., K.T., S.O., I.S., M.Y., A.N., I.K.), Chiba University Graduate School of Medicine, Chiba, Japan; PRESTO (T.M.), Japan Science and Technology Agency, Saitama, Japan; Division of Vascular Biology (A.U.), Department of Physiology and Cell Biology, Kobe University Graduate School of Medicine, Japan; Laboratory for Stem Cell Biology (M.O.), RIKEN Center for Developmental Biology, Kobe, Japan; and Laboratory of Medical Genomics (H.K.), Department of Human Genome Research, Kazusa DNA Research Institute, Chiba, Japan.

*Both authors contributed equally to this work.

Correspondence to Issei Komuro, MD, PhD, Department of Cardiovascular Science and Medicine, Chiba University Graduate School of Medicine, 1-8-1 Inohana, Chuo-ku, Chiba 260-8670, Japan. E-mail komuro-tky@umin.ac.jp

Circulation Research **is available at http://circres.ahajournals.org** **DOI: 10.1161/CIRCRESAHA.109.210815**

Non-standard Abbreviations and Acronyms	
ERK	extracellular signal-regulated kinase
HUVEC	human umbilical vein endothelial cell
Sema	semaphorin
VEGF	vascular endothelial growth factor
VEGFR	vascular endothelial growth factor receptor

In this study, we performed both in vivo and in vitro investigations into the role of Sema3E/plexinD1 in postnatal angiogenesis, and we found that these 2 molecules inhibit angiogenesis by suppressing the vascular endothelial growth factor (VEGF) signaling pathway. Sema3E expression was upregulated in ischemic tissue via a p53-dependent pathway. Its upregulation was further enhanced in a diabetic model, attenuating the effect of VEGF treatment, whereas inhibition of Sema3E markedly improved the response to VEGF. These findings suggest that inhibition of Sema3E may be a novel strategy for therapeutic angiogenesis, especially when VEGF is ineffective.

Methods

Cell Culture

Recombinant human VEGF165 (293-VE), monoclonal antihuman VEGF antibody (MAB293) and recombinant human Sema3E were purchased from R&D Systems (Minneapolis, Minn). PlexinD1 Fc protein was generated by ARK Resource (Kumamoto, Japan). Human umbilical vein endothelial cells (HUVECs) were purchased from BioWhittaker (Walkersville, Md) and cultured according to the instructions of the manufacturer. Endothelial cell proliferation was assessed by determining cell counts after culture in the presence of VEGF165 (50 ng/mL) for 2 days. Retroviral stocks were generated by transient transfection of packaging cell line (PT67, Clontech) and stored at −80°C until use. Human endothelial cells (passage 4 to 6) were plated at 5×10^5 cells per 100-mm-diameter dish 24 hours before infections. For infections, the culture medium was replaced by retroviral stocks supplemented with 8 μg/mL polybrene (Sigma, Tokyo, Japan). Forty-eight hours after infections, the infected cell populations were selected by culture in 0.8 μg/mL puromycin for 4 days. High-titer adenoviral stocks (10^9 pfu) were generated with the Adeno-X Expression System (Clontech) according to the instructions of the manufacturer.

Tube-Formation Assay

The tube-formation assay was performed using a commercially available kit according to the manufacturer's instructions (Kurabo, Osaka, Japan). HUVECs were cultured for 11 days in the presence of VEGF165 (10 ng/mL) and test substances, after which they were fixed at room temperature in 70% ethanol. The fixed cells were then incubated first with mouse antihuman CD31 antibody (1:4000 dilution) for 1 hour and then with a goat anti-mouse IgG alkaline phosphatase–conjugated secondary antibody, which was visualization using 5-bromo-4-chloro-3-indolyl phosphate/nitro blue tetrazolium. Capillary-like tube formation was assessed by photography under an inverted phase contrast microscope at a ×40 magnification. The vessel area was defined as the area of CD31-positive cells / total area, which was estimated by an angiogenesis image analyzer (Kurabo, Osaka, Japan). This assay was performed in triplicate.

Western Blot Analysis

Whole cell lysates were prepared in lysis buffer (10 mmol/L Tris-HCl, pH 8, 140 mmol/L NaCl, 5 mmol/L EDTA, 0.025% NaN3, 1% Triton X-100, 1% deoxycholate, 0.1% SDS, 1 mmol/L PMSF, 5 μg/mL leupeptin, 2 μg/mL aprotinin, 50 mmol/L NaF, and 1 mmol/L Na_2VO_3). The lysates (30 to 50 μg) were resolved by SDS-PAGE. Proteins were transferred to a poly(vinylidene difluoride) membrane (Millipore, Bedford, Mass) and incubated with the primary antibody followed by anti-rabbit IgG–horseradish peroxidase antibody or anti-mouse IgG–horseradish peroxidase antibody or anti-goat IgG–horseradish peroxidase antibody (Jackson, West Grove, Pa). Specific proteins were detected by using enhanced chemiluminescence (Amersham, Buckinghamshire, UK). Immunoprecipitation was performed as described previously.[15] The primary antibodies used for Western blotting were as follows; anti–phospho–extracellular signal-regulated kinase (ERK) antibody (sc-7383), anti-ERK antibody (sc-154-G), anti-pAkt antibody (sc-7985-R), anti-Akt antibody (sc-1618), anti-p53 antibody (sc-126, sc-99), anti-actin antibody (sc-8432), anti–flk-1 antibody (sc-6251), anti-Sema3E antibody (sc-49733) (Santa Cruz Biotechnology, Santa Cruz, Calif), and anti-phosphotyrosine antibody (4G10) (Upstate, Lake Placid, NY). All immunoblotting analyses were performed more than three times.

RNA Analysis

Total RNA (30 μg) was extracted by the guanidinium thiocyanate-phenol chloroform method using RNA zol B (Tel Test, Friendswood, Tex) according to the instructions of the manufacturer. cDNA was prepared using the SuperScript First-Strand Synthesis System for RT-PCR (Invitrogen). Quantitative real-time PCR was performed by using the LightCycler (Roche, Indianapolis, Ind) with the TaqMan Universal ProbeLibrary and the LightCycler Master (Roche) according to the instructions of the manufacturer.

Experimental Animals

The animal experiments were approved by our institutional review board. C57/BL6 mice were purchased from the SLC Japan. All mice used in this study were 8 to 12 weeks old. p53-deficient mice (in C57/BL6 background) were purchased from The Jackson Laboratory (Bar Harbor, Me). For the type 1 diabetic model, mice were treated with an intraperitoneal injection of streptozotocin in 0.1 mol/L sodium citrate (pH 4.5) at a dose of 50 mg/kg body weight for 5 days. Generation and genotyping of Sema3E-deficient mice (in C57/BL6 background) have been described previously.[10]

Hindlimb Ischemia Model

After mice were anesthetized, the proximal part of the femoral artery and the distal portion of the popliteal artery were ligated and stripped out after all side branches were dissected free.[16] For in vivo gene transfer, we exposed thigh muscle by excising the skin and injected the expression vector encoding soluble plexinD1-Fc, VEGF, or Sema3E into the muscle twice after surgery. We analyzed blood flow recovery until day 28 after surgery. Hindlimb perfusion was measured with a laser Doppler perfusion analyzer (Moor Instruments, Devon, UK). Ischemic limb samples were harvested for histology on day 10 after surgery. Vastus and rectus femoris muscle tissues were removed from the ischemic limbs after systemic perfusion with PBS and immediately embedded in OCT compound (Sakura Finetechnical). Then, each specimen was snap frozen in liquid nitrogen and cut into 6 μm sections. The sections were stained with antibodies for CD31 (Pharmingen), plexinD1, or Sema3E (Santa Cruz Biotechnology). Two transverse sections of the entire muscle were photographed digitally at a magnification of ×100 (12 to 16 photographs per mouse), and these photographs were reviewed in a blinded manner. Capillary endothelial cells were identified by immunoreactivity for CD31 and quantified as vessel area (%), which was defined as the area of CD31-positive cells/total area.

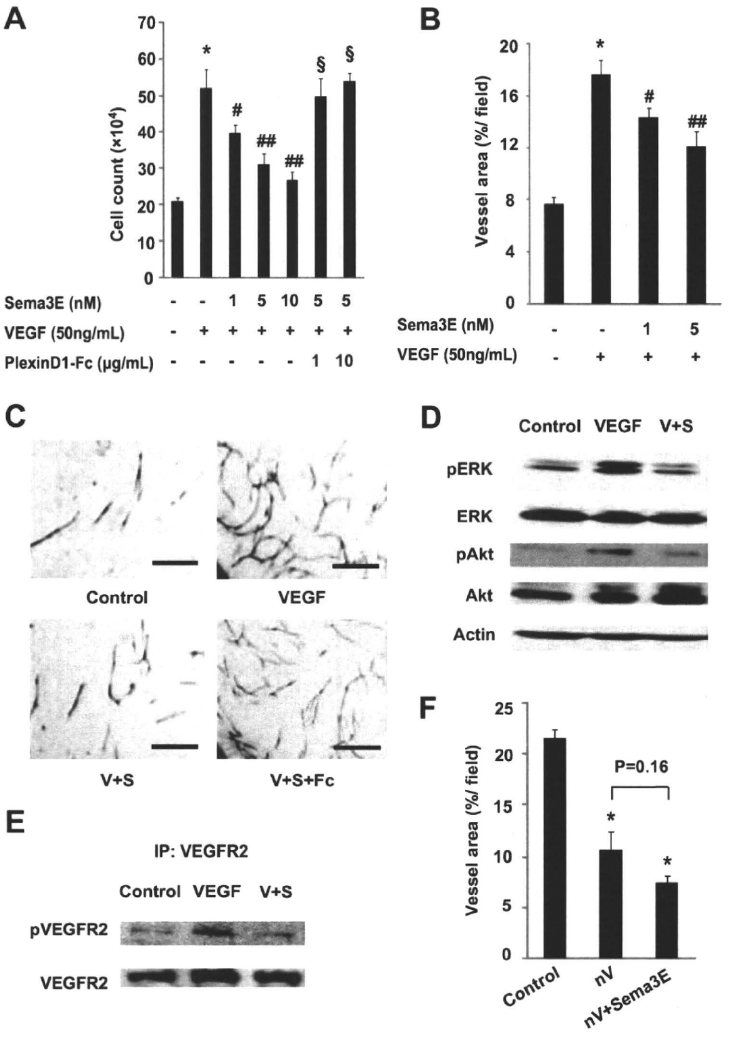

Figure 1. Sema3E suppresses VEGF-induced angiogenesis. A, Cultured endothelial cells were treated with VEGF alone (50 ng/mL) or VEGF+Sema3E (1, 5, or 10 nmol/L) or VEGF+Sema3E+plexinD1-Fc (1 or 10 μg/mL). Sema3E significantly inhibited VEGF-induced endothelial cell proliferation, which was effectively reversed by plexinD1-Fc treatment. *$P<0.01$ vs Sema3E (−)/VEGF (−)/plexinD1-Fc (−) (n=4); #$P<0.05$, ##$P<0.01$ vs Sema3E (−)/VEGF (+)/plexinD1-Fc (−) (n=4); §$P<0.01$ vs Sema3E (5 nmol/L)/VEGF (+)/plexinD1-Fc (−) (n=4). Data represent means±SEM. B, Endothelial cells cocultured with fibroblasts were treated with VEGF and/or Sema3E for 11 days, and vessel area was assayed by immunohistochemistry for CD31. Sema3E significantly inhibited VEGF-induced tube formation. *$P<0.01$ vs Sema3E (−)/VEGF (−) (n=4); #$P<0.05$, ##$P<0.01$ vs Sema3E (−)/VEGF (+) (n=4). Data represent means±SEM. C, Photographs show tube formation of endothelial cells in the presence of VEGF (50 ng/mL) (VEGF), VEGF+Sema3E (5 nmol/L) (V+S), or VEGF+Sema3E+PlexinD1-Fc (10 μg/mL) (V+S+Fc). Scale bar=300 μm. Vehicle treatment served as control (control). D, Endothelial cells were treated with VEGF (50 ng/mL) (VEGF) or VEGF plus Sema3E (5 nmol/L) (V+S) and analyzed for the VEGF signal pathways by Western blot analysis (n=4). Sema3E suppressed VEGF-induced phosphorylation of ERK (pERK) and Akt (pAkt). Vehicle treatment served as control (control). E, Protein samples prepared in D were analyzed for phospho-VEGFR2 levels (n=7). Sema3E suppressed VEGF-induced phosphorylation of VEGFR2. F, VEGF-induced tube formation was examined in the presence of anti-VEGF antibody (500 μg/mL) (nV), Sema3E (5 nmol/L) (Sema3E), or anti-VEGF antibody plus Sema3E (nV+Sema3E). Vehicle treatment served as control (control). In the presence of anti-VEGF antibody, Sema3E did not significantly inhibit tube formation. *$P<0.01$ vs control (n=4).

Statistical Analysis

Data were shown as means±SEM. Multiple group comparison was performed by 1-way ANOVA followed by the Bonferroni procedure for comparison of means. Comparisons between 2 groups were analyzed by the unpaired Student t test. Values of $P<0.05$ were considered statistically significant.

Results

Sema3E Suppresses VEGF-Induced Angiogenesis in Cultured Endothelial Cells

To investigate the role of Sema3E/plexinD1, we first performed an in vitro study using HUVECs. We seeded HUVECs at 1×10^5 cells per 100-mm-diameter dish and counted the number of cells at 2 days after seeding. Treatment of HUVECs with VEGF markedly increased the cell count (Figure 1A), although this increase was strongly inhibited by addition of Sema3E in a dose-dependent manner (Figure 1A). Treatment with a plexinD1-Fc fusion protein, which binds to Sema3E and inhibits its activity, blocked the effect of Sema3E (Figure 1A). We also performed an angiogenesis assay, in which HUVECs were cocultured with fibroblasts in the presence or absence of Sema3E. When endothelial tube formation was assessed after 11 days, it was found that treatment with VEGF markedly increased tube formation, although this increase was significantly inhibited by addition of Sema3E (Figure 1B). Treatment with the plexinD1-Fc fusion protein also antagonized the effect of Sema3E on VEGF-induced tube formation (Figure 1C), suggesting that Sema3E is an antiangiogenic factor. We next investigated how Sema3E inhibited angiogenesis. After depriving HUVECs of VEGF for 7 hours, we examined the effect of VEGF treatment. Addition of VEGF induced the phosphorylation of ERK and Akt, both of which are crucial kinases in the intracellular signaling pathway for this growth factor. Pretreatment with Sema3E suppressed VEGF-induced phosphorylation of these two kinases (Figure 1D; Online Figure I, A). Sema3E treatment also suppressed VEGF-induced phosphorylation of VEGF receptor (VEGFR)-2 (Figure 1E; Online Figure I, B). To determine whether the antiangiogenic effect of Sema3E was VEGF-dependent, we next examined the response to addition of an anti-VEGF neutralizing antibody. In the presence of the anti-VEGF antibody, Sema3E did not significantly inhibit cell growth and tube formation (Figure 1F; Online Figure I, C),

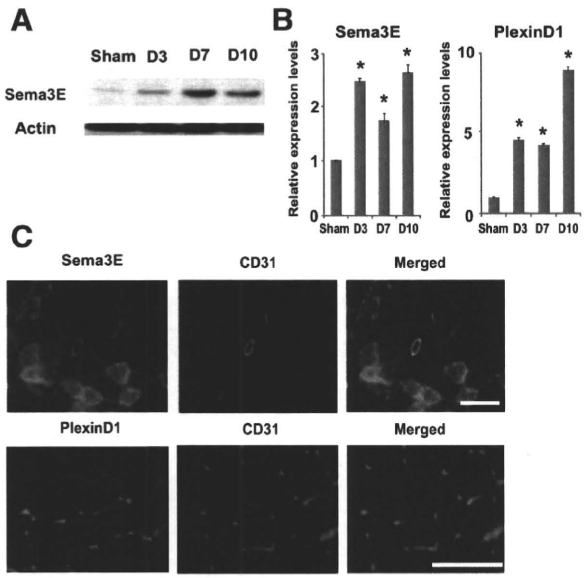

Figure 2. Expression of Sema3E is markedly upregulated in ischemic tissues. A, Western blot analysis for Sema3E expression in ischemic limbs on day 3 (D3), day 7 (D7), and day 10 (D10) after surgery (n=5). Sham indicates sham-operated. B, The mRNA levels of Sema3E and plexinD1 in ischemic limbs on day 3 (D3), day 7 (D7), and day 10 (D10) after surgery were assessed by real-time PCR analysis. *$P<0.01$ vs sham (n=5). Data represent means±SEM. C, The frozen sections of murine ischemic tissue on day 10 after surgery were subjected to immunofluorescence staining for Sema3E (top) or plexinD1 (bottom) (green). The sections were double-stained with CD31 (red). Scale bar=100 μm.

suggesting that Sema3E negatively regulates angiogenesis by inhibiting the VEGF pathway.

Sema3E Suppresses Angiogenesis In Vivo

To investigate the role of Sema3E/plexinD1 in postnatal angiogenesis, we used a murine model of hindlimb ischemia that was created by unilateral femoral artery ligation. Ischemic tissues were harvested and subjected to Western blot analysis and immunohistochemistry. Expression of Sema3E and plexinD1 was markedly increased in ischemic limbs at 3 days after surgery, and this increase persisted until day 10 (Figure 2A and 2B; Online Figure II). Immunohistochemistry showed that Sema3E was expressed by arterioles, myocytes, and capillary endothelial cells in the ischemic limbs, whereas plexinD1 was mainly expressed by capillary endothelial cells (Figure 2C). To examine whether inhibition of Sema3E promoted angiogenesis, we injected an expression vector encoding the plexinD1-Fc gene into ischemic limbs and analyzed blood flow recovery and the vessel area of the limbs. Laser Doppler perfusion imaging revealed that the plexinD1-Fc group showed significantly better recovery of blood flow than the control group (Figure 3A). Likewise, the vessel area of ischemic limbs at 10 days after surgery was significantly larger in the plexinD1-Fc group than in the control group (Figure 3B; Online Figure III, A).

To further investigate the effect of Sema3E on angiogenesis, we introduced an expression vector encoding the VEGF gene, a vector for the Sema3E gene, or the vectors for both genes. Injection of the VEGF vector into ischemic limbs significantly accelerated blood flow recovery compared with the control group, whereas this effect was suppressed by coinjection of the Sema3E vector (Figure 3C). In addition, the vessel area was smaller in the Sema3E plus VEGF group than in the VEGF alone group (Figure 3C). Moreover, injection of a vector encoding the plexinD1-Fc gene into ischemic limbs treated with the Sema3E and VEGF vectors significantly improved blood flow recovery and increased the vessel area compared with the findings in the Sema3E plus VEGF group (Figure 3C), suggesting that Sema3E also inhibits neovascularization in ischemic tissue. Next, we created hindlimb ischemia in Sema3E-deficient mice to examine the effect of loss-of-function of this molecule. Consistent with the results of our gene transfer experiments, Sema3E-deficient mice[10] showed better blood flow recovery and a larger vessel area in their ischemic limbs than wild-type mice (Figure 3D; Online Figure III, B). These results indicate that Sema3E/plexinD1 negatively regulate postnatal angiogenesis.

p53 Upregulates Sema3E Expression Both In Vitro and In Vivo

There is evidence that expression of the tumor suppressor protein p53 is increased by hypoxia, thereby inhibiting tumor angiogenesis.[17,18] We identified a putative p53-binding element within the promoter region of the Sema3E gene (data not shown), suggesting that induction of p53 by hypoxia might upregulate Sema3E expression in ischemic limbs. To investigate this hypothesis, we infected HUVECs with an adenoviral vector encoding p53, and then examined Sema3E expression by Western blot analysis. In agreement with our hypothesis, overexpression of p53 led to upregulation of Sema3E expression in HUVECs (Figure 4A). Expression of Sema3E was also induced by treatment with cobalt chloride, which mimics the effects of hypoxia (Figure 4B). To further investigate the relationship between p53 and Sema3E, we next infected HUVECs with a retroviral vector encoding the HPV16 E6 gene, which blocks p53 expression and examined the effect on expression of Sema3E by endothelial cells. Exposure to cobalt chloride for 12 hours markedly upregulated both Sema3E and p53 expression in mock-infected HUVECs, whereas there was no induction of Sema3E expression in E6-infected cells (Figure 4B), suggesting that hypoxia promoted the induction of Sema3E via a p53-dependent pathway.

Consistent with our in vitro data, expression of both p53 and Sema3E was markedly increased in the ischemic limbs of wild-type mice at 3 days after femoral artery ligation (Figures 2A and 4C; Online Figure IV, A). To determine whether Sema3E was regulated by p53 in vivo, we created hindlimb ischemia in p53-deficient mice and wild-type mice and then examined the expression of Sema3E in ischemic limbs. Consistent with our in vitro results, upregulation of Sema3E expression was abolished in the ischemic limbs of p53-deficient mice (Figure 4D; Online Figure IV, B), suggesting that an increase of p53 promotes Sema3E expression in ischemic tissue and thus inhibits blood flow recovery.

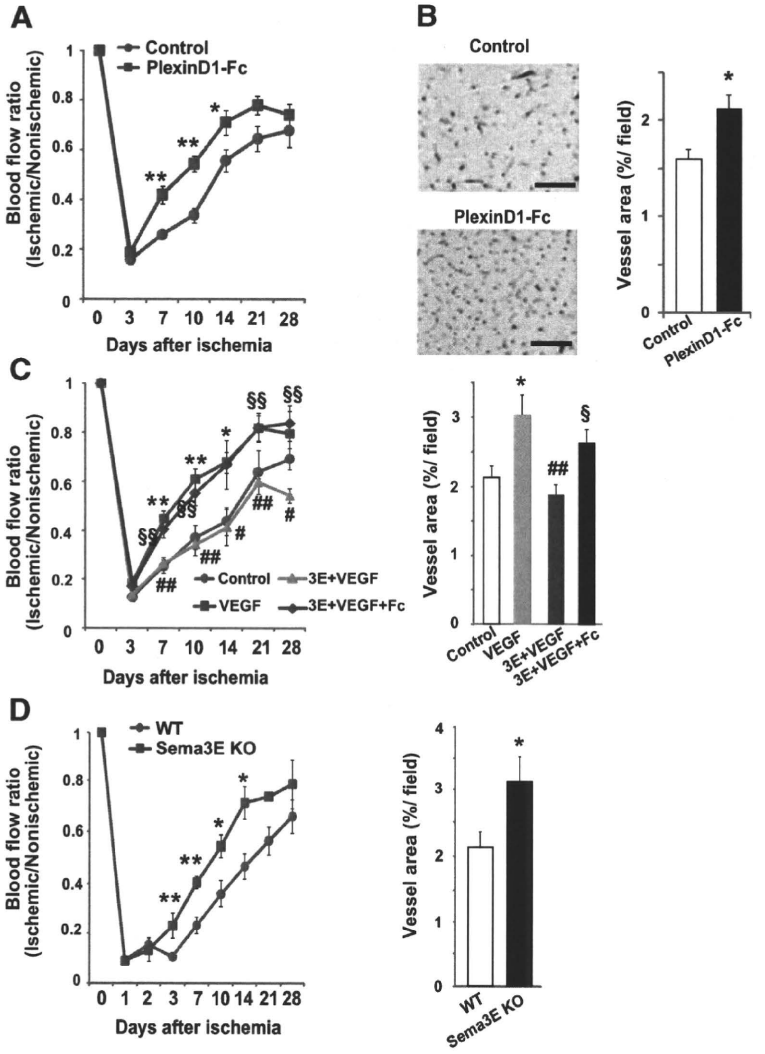

Figure 3. Sema3E negatively regulates angiogenesis in ischemic tissue. A and B, Ischemic limbs of mice were treated with an empty vector (control) or the plexinD1-Fc expression vector (plexinD1-Fc) by intramuscular injection, and blood flow recovery (A) and vessel area (B) were analyzed by laser Doppler perfusion imaging and immunohistochemistry for CD31, respectively. Mice treated with plexinD1-Fc showed better blood flow recovery and a larger vessel area. *$P<0.05$, **$P<0.01$ vs control (n=8 for A and B). Data represent means±SEM. Photographs show immunohistochemistry for CD31 in ischemic limbs on 10 days after surgery. Scale bar=100 μm. C, Ischemic limbs of mice were treated with mock (control), the VEGF vector only (VEGF), the Sema3E and VEGF vectors (3E+VEGF), or the Sema3E, VEGF, and plexinD1-Fc vectors (3E+VEGF+Fc), and blood flow recovery (left) and vessel area (right) were analyzed by laser Doppler perfusion imaging and CD31 immunohistochemistry, respectively. Injection of the Sema3E vector into ischemic limbs suppressed VEGF-induced neovascularization, which was effectively reversed by the plexinD1-Fc vector treatment. *$P<0.05$, **$P<0.01$ vs control; #$P<0.05$, ##$P<0.01$ vs VEGF; §$P<0.05$, §§$P<0.01$ vs 3E+VEGF (n=8 to 10). Data represent means±SEM. D, Ischemic limbs of wild-type mice (WT) and Sema3E-deficient mice (Sema3E KO) were analyzed for blood flow recovery (left) and vessel area (right). Sema3E-deficient mice showed better blood flow recovery and a larger vessel area of ischemic limbs. *$P<0.05$ vs WT mice (n=3 to 8). Data represent means±SEM.

Inhibition of Sema3E Improves Angiogenesis in Diabetic Mice

It has been reported that the angiogenic response to ischemia is attenuated in patients with diabetes.[19] We created a murine model of type 1 diabetes by intraperitoneal injection of streptozotocin (50 mg/kg per day for 5 days) and examined neovascularization after the animals were subjected to hind-limb ischemia. Blood glucose level was significantly higher and blood insulin level was significantly lower in streptozotocin-induced diabetic mice than in control mice (Online Figure V, A). Mice with streptozotocin-induced diabetes also showed poor blood flow recovery and a smaller vessel area in their ischemic limbs compared with control mice (Figure 5A and 5B). To investigate whether the impairment of neovascularization in diabetic mice was related to p53 and Sema3E, we examined the expression of these proteins in the mice. Western blot analysis revealed that p53 expression was increased in diabetic mice and that this increase was further enhanced by ischemia (Figure 5C; Online Figure V, B; and data not shown). Likewise, expression of Sema3E was significantly increased in diabetic mice compared with control mice (Figure 5C; Online Figure V, B). Consequently, blood flow recovery and the increase of the vessel area after VEGF treatment were significantly impaired in diabetic mice compared with VEGF-treated control mice (Figure 5A and 5B). To further assess the effect of inhibition of Sema3E in diabetic mice, we injected an expression vector encoding the plexinD1-Fc gene into the ischemic limbs of diabetic mice. Laser Doppler perfusion imaging of ischemic limbs and immunohistochemistry for CD31 revealed that the poor response of neovascularization to VEGF treatment was effectively overcome by introduction of the plexinD1-Fc gene (Figure 5D), suggesting that overexpression of Sema3E was responsible for impairment of neovascularization in the diabetic mice. These results indicate that inhibition of Sema3E is effective for promoting angiogenesis, especially when VEGF treatment is ineffective, such as in the diabetic state.

Discussion

The present study demonstrated that the Sema3E/plexinD1 axis inhibits postnatal angiogenesis in a murine model of

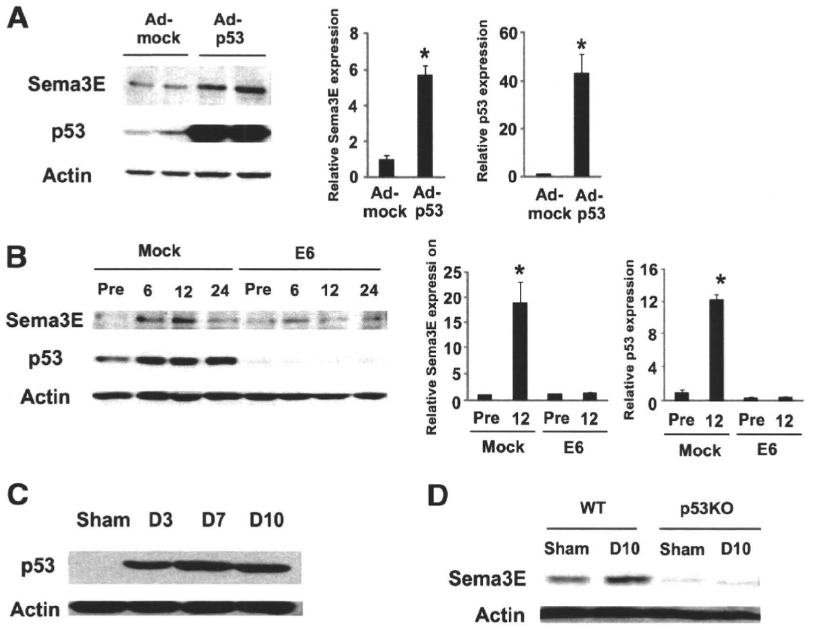

Figure 4. p53 regulates expression of Sema3E. A, Endothelial cells were infected with an adenoviral vector encoding p53 (Ad-p53) or mock (Ad-mock) and subjected to Western blot analysis for expression of Sema3E and p53 (left). Relative expression levels of Sema3E and p53 were plotted in the graph (right). *$P<0.01$ vs Ad-mock (n=4). Overexpression of p53 upregulated Sema3E expression. B, Endothelial cells were infected with a retroviral vector encoding HPV16 E6 (E6) or mock (Mock) and treated with $CoCl_2$ (100 μmol/L) for 6, 12, 24 hours (6, 12, 24). Expression of Sema3E and p53 was examined by Western blot analysis (left). Relative expression levels of Sema3E and p53 were plotted in the graph (right). *$P<0.05$ vs control (Pre) (n=3). Treatment with $CoCl_2$ markedly upregulated Sema3E expression compared to control (Pre), and this upregulation was inhibited by disruption of p53. C, Western blot analysis for p53 expression on day 3 (D3), day 7 (D7), and day 10 (D10) after surgery (n=4). Sham indicates sham-operated. Expression of p53 was markedly upregulated 3 days after surgery, and this upregulation persisted for 10 days. D, Western blot analysis for Sema3E expression in ischemic limbs of wild-type (WT) or p53-deficient (p53KO) mice on day 10 after surgery (n=4). Sema3E expression was increased in ischemic limbs of wild-type mice but not p53-deficient mice.

hindlimb ischemia. Our results also suggested that Sema3E inhibits angiogenesis by blocking activation of the VEGFR-2 and its downstream signaling pathway. Although Sema3E does not bind to neuropilin-1,[10] attraction of axons by Sema3E requires the presence of neuropilin-1 in addition to plexinD1, so the mode of assembly of the ligand and receptor complex is thought to determine the function of Sema3E.[20] Neuropilin-1 also binds to the VEGFR-2 and plays a crucial role in the regulation of VEGF signaling.[21] Accordingly, Sema3E may inhibit VEGF-induced angiogenesis by limiting the availability of neuropillin-1. Because treatment with an anti-VEGF neutralizing antibody did not completely over-

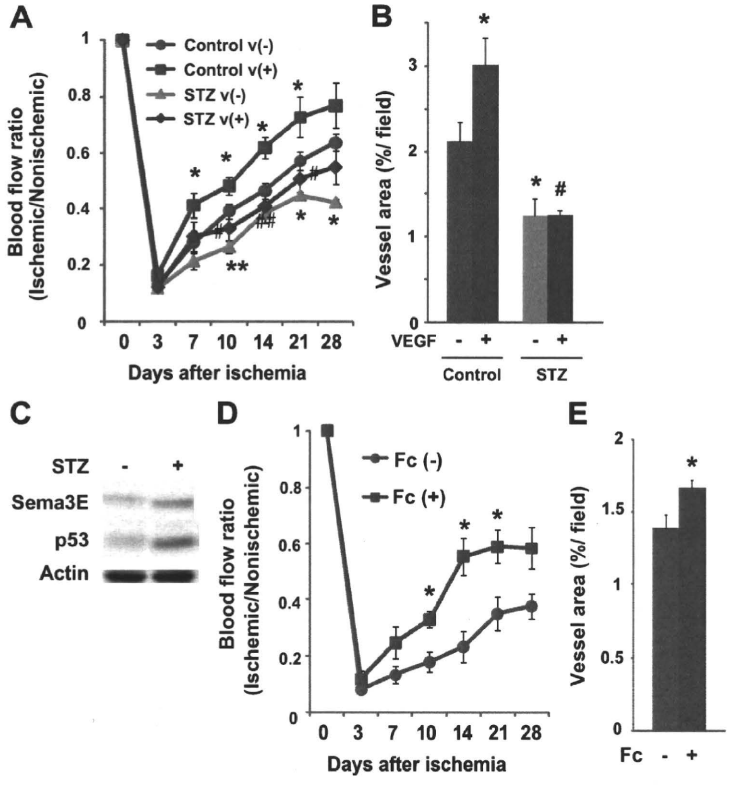

Figure 5. Sema3E inhibition improves impaired angiogenesis in diabetic mice. A and B, Blood flow recovery (A) and vessel area (B) in ischemic limbs of control (control) or streptozotocin-induced diabetic (STZ) mice after treatment with mock [v(−)] or the VEGF expression vector [v(+)]. Diabetic mice showed impaired blood recovery and a smaller vessel area in ischemic limbs compared with control mice. They showed less response to VEGF treatment. *$P<0.05$, **$P<0.01$ vs control/v(−); #$P<0.05$, ##$P<0.01$ vs control/v(+) (n=5 to 12). Data represent means±SEM. C, Expression of Sema3E and p53 was examined in limb tissues of control (STZ−) and streptozotocin-induced diabetic mice (STZ+) by Western blot analysis (n=4). Expression of Sema3E and p53 was upregulated in diabetic mice. D and E, Blood flow recovery (D) and vessel area (E) were analyzed in ischemic limbs of diabetic mice treated with VEGF [Fc(−)] or VEGF+plexinD1-Fc [Fc(+)]. Treatment of plxinD1-Fc in addition to VEGF significantly improved neovascularization in diabetic mice. *$P<0.01$ vs Fc(−) (n=7 to 9). Data represent means±SEM.

come the inhibitory effect of Sema3E on angiogenesis, this effect may also be attributable to the signaling pathway downstream of Sema3E-plexinD1, which is currently unknown.

Sema3E suppressed VEGF-induced phosphorylation of ERK and Akt (Figure 1D). It is well accepted that both ERK and Akt are crucial for the intracellular signaling pathways stimulated by hepatocyte growth factor (HGF) or basic fibroblast growth factor basic (bFGF) to induce angiogenesis. Interestingly, Sema3E also inhibited bFGF or HGF-induced tube formation in a dose-dependent manner (Online Figure VI, A). Moreover, Sema3E significantly inhibited bFGF-induced tube formation even in the presence of the anti-VEGF antibody, whereas it did not inhibit HGF-induced tube formation (Online Figure VI, B). These results suggest that besides the suppression of VEGF-induced angiogenesis, the antiangiogenic effect of Sema3E was partially mediated by VEGF-independent mechanisms.

It is known that intersomitic vessels are disorganized in Sema3E-deficient mice,[10] and this phenotype is markedly similar to that observed in mice lacking plexinD1.[13,14] However, whereas plexinD1-deficient mice develop severe cardiovascular defects involving the outflow tract of the heart and derivatives of the aortic arch arteries that result in perinatal death,[13] Sema3E-deficient mice do not show any large vessel abnormalities and do not undergo embryonic death. PlexinD1 has also been reported to bind to other semaphorins besides Sema3E, such as Sema3A,[13] Sema3C,[22] and Sema4A.[23] It has been shown that Sema3E only binds to plexinD1, whereas Sema3A and Sema3C bind to plexinA1 as well as to plexinD1.[5,10] Sema3A-deficient mice show neural path-finding defects and abnormalities of vascular development that result in neonatal death.[24–26] Ablation of the Sema3C gene in mice results in severe outflow tract abnormalities and mispatterning of intersomitic vessels.[27] Because plexinA1 deficiency also leads to cardiovascular defects,[28] Sema3A/C may play a pivotal role in embryonic vascular development regulated by the plexinA1/D1 pathway. More recently, Sema3A and Sema4A have been shown to inhibit postnatal angiogenesis,[29] suggesting that plexinD1-Fc treatment increases blood flow recovery in ischemic limbs by inhibiting Sema3E but also Sema3A/4A. Sema4D also has an inhibitory effect on postnatal angiogenesis[30]; however, it remains to be determined whether Sema4D binds to plexinD1.

Our results further suggest that p53 has a crucial role in the induction of Sema3E expression in ischemic tissue, although the precise mechanism of how p53 regulates Sema3E expression remains unknown. Because the antiangiogenic activity of p53 is important for tumor suppression, Sema3E/plexinD1 could be a potential target for the treatment of malignancies with p53 mutations. It has been reported that hyperglycemia activates p53 by increasing the production of reactive oxygen species.[31] Thus, p53-induced upregulation of antiangiogenic factors (including Sema3E) is likely to account for the impairment of angiogenesis in patients with diabetes. Therefore, Sema3E/plexinD1 could also be a target for the treatment of ischemic cardiovascular disease in diabetic patients because conventional therapeutic angiogenesis is not very efficient in this patient population.[32,33]

Acknowledgment

We thank Christopher Henderson, Columbia University, New York, for providing us with Sema3E knockout mice.

Sources of Funding

This work was supported by a Grant-in-Aid for Scientific Research from the Ministry of Education, Science, Sports, and Culture and Health and Labor Sciences Research Grants (to I.K.); a Grant-in-Aid for Scientific Research from the Ministry of Education, Culture, Sports, Science and Technology of Japan and grants from the Suzuken Memorial Foundation, the Japan Diabetes Foundation, the Ichiro Kanehara Foundation, the Tokyo Biochemical Research Foundation, the Takeda Science Foundation, the Cell Science Research Foundation, and the Japan Foundation of Applied Enzymology (to T.M.).

Disclosures

None.

References

1. Carmeliet P, Tessier-Lavigne M. Common mechanisms of nerve and blood vessel wiring. *Nature*. 2005;436:193–200.
2. Dickson BJ. Molecular mechanisms of axon guidance. *Science*. 2002; 298:1959–1964.
3. Weinstein BM. Vessels and nerves: marching to the same tune. *Cell*. 2005;120:299–302.
4. Eichmann A, Le Noble F, Autiero M, Carmeliet P. Guidance of vascular and neural network formation. *Curr Opin Neurobiol*. 2005;15:108–115.
5. Neufeld G, Kessler O. The semaphorins: versatile regulators of tumour progression and tumour angiogenesis. *Nat Rev Cancer*. 2008;8:632–645.
6. Luo Y, Raible D, Raper JA. Collapsin: a protein in brain that induces the collapse and paralysis of neuronal growth cones. *Cell*. 1993;75:217–227.
7. Tamagnone L, Artigiani S, Chen H, He Z, Ming GI, Song H, Chedotal A, Winberg ML, Goodman CS, Poo M, Tessier-Lavigne M, Comoglio PM. Plexins are a large family of receptors for transmembrane, secreted, and GPI-anchored semaphorins in vertebrates. *Cell*. 1999;99:71–80.
8. Ohta K, Mizutani A, Kawakami A, Murakami Y, Kasuya Y, Takagi S, Tanaka H, Fujisawa H. Plexin: a novel neuronal cell surface molecule that mediates cell adhesion via a homophilic binding mechanism in the presence of calcium ions. *Neuron*. 1995;14:1189–1199.
9. Song H, Ming G, He Z, Lehmann M, McKerracher L, Tessier-Lavigne M, Poo M. Conversion of neuronal growth cone responses from repulsion to attraction by cyclic nucleotides. *Science*. 1998;281:1515–1518.
10. Kruger RP, Aurandt J, Guan KL. Semaphorins command cells to move. *Nat Rev Mol Cell Biol*. 2005;6:789–800.
11. Roth L, Koncina E, Satkauskas S, Cremel G, Aunis D, Bagnard D. The many faces of semaphorins: from development to pathology. *Cell Mol Life Sci*. 2009;66:649–666.
12. Christensen CR, Klingelhofer J, Tarabykina S, Hulgaard EF, Kramerov D, Lukanidin E. Transcription of a novel mouse semaphorin gene, M-semaH, correlates with the metastatic ability of mouse tumor cell lines. *Cancer Res*. 1998;58:1238–1244.
13. Gitler AD, Lu MM, Epstein JA. PlexinD1 and semaphorin signaling are required in endothelial cells for cardiovascular development. *Dev Cell*. 2004;7:107–116.
14. Torres-Vazquez J, Gitler AD, Fraser SD, Berk JD, Van NP, Fishman MC, Childs S, Epstein JA, Weinstein BM. Semaphorin-plexin signaling guides patterning of the developing vasculature. *Dev Cell*. 2004;7:117–123.
15. Minamino T, Mitsialis SA, Kourembanas S. Hypoxia extends the life span of vascular smooth muscle cells through telomerase activation. *Mol Cell Biol*. 2001;21:3336–3342.
16. Couffinhal T, Silver M, Zheng LP, Kearney M, Witzenbichler B, Isner JM. Mouse model of angiogenesis. *Am J Pathol*. 1998;152:1667–1679.
17. Harris SL, Levine AJ. The p53 pathway: positive and negative feedback loops. *Oncogene*. 2005;24:2899–2908.
18. Teodoro JG, Parker AE, Zhu X, Green MR. p53-mediated inhibition of angiogenesis through up-regulation of a collagen prolyl hydroxylase. *Science*. 2006;313:968–971.

19. Falanga V. Wound healing and its impairment in the diabetic foot. *Lancet.* 2005;366:1736–1743.
20. Chauvet S, Cohen S, Yoshida Y, Fekrane L, Livet J, Gayet O, Segu L, Buhot MC, Jessell TM, Henderson CE, Mann F. Gating of Sema3E/PlexinD1 signaling by neuropilin-1 switches axonal repulsion to attraction during brain development. *Neuron.* 2007;56:807–822.
21. Soker S, Takashima S, Miao HQ, Neufeld G, Klagsbrun M. Neuropilin-1 is expressed by endothelial and tumor cells as an isoform-specific receptor for vascular endothelial growth factor. *Cell.* 1998;92:735–745.
22. Banu N, Teichman J, Dunlap-Brown M, Villegas G, Tufro A. Semaphorin 3C regulates endothelial cell function by increasing integrin activity. *FASEB J.* 2006;20:2150–2152.
23. Toyofuku T, Yabuki M, Kamei J, Kamei M, Makino N, Kumanogoh A, Hori M. Semaphorin-4A, an activator for T-cell-mediated immunity, suppresses angiogenesis via Plexin-D1. *EMBO J.* 2007;26:1373–1384.
24. Behar O, Golden JA, Mashimo H, Schoen FJ, Fishman MC. Semaphorin III is needed for normal patterning and growth of nerves, bones and heart. *Nature.* 1996;383:525–528.
25. Taniguchi M, Yuasa S, Fujisawa H, Naruse I, Saga S, Mishina M, Yagi T. Disruption of semaphorin III/D gene causes severe abnormality in peripheral nerve projection. *Neuron.* 1997;19:519–530.
26. Serini G, Valdembri D, Zanivan S, Morterra G, Burkhardt C, Caccavari F, Zammataro L, Primo L, Tamagnone L, Logan M, Tessier-Lavigne M, Taniguchi M, Puschel AW, Bussolino F. Class 3 semaphorins control vascular morphogenesis by inhibiting integrin function. *Nature.* 2003;424:391–397.
27. Feiner L, Webber AL, Brown CB, Lu MM, Jia L, Feinstein P, Mombaerts P, Epstein JA, Raper JA. Targeted disruption of semaphorin 3C leads to persistent truncus arteriosus and aortic arch interruption. *Development.* 2001;128:3061–3070.
28. Toyofuku T, Zhang H, Kumanogoh A, Takegahara N, Suto F, Kamei J, Aoki K, Yabuki M, Hori M, Fujisawa H, Kikutani H. Dual roles of Sema6D in cardiac morphogenesis through region-specific association of its receptor, Plexin-A1, with off-track and vascular endothelial growth factor receptor type 2. *Genes Dev.* 2004;18:435–447.
29. Maione F, Molla F, Meda C, Latini R, Zentilin L, Giacca M, Seano G, Serini G, Bussolino F, Giraudo E. Semaphorin 3A is an endogenous angiogenesis inhibitor that blocks tumor growth and normalizes tumor vasculature in transgenic mouse models. *J Clin Invest.* 2009;119:3356–3372.
30. Sun Q, Zhou H, Binmadi NO, Basile JR. Hypoxia inducible factor-1-mediated regulation of Semaphorin 4D affects tumor growth and vascularity. *J Biol Chem.* 2009;284:32066–32074.
31. Brodsky SV, Gealekman O, Chen J, Zhang F, Togashi N, Crabtree M, Gross SS, Nasjletti A, Goligorsky MS. Prevention and reversal of premature endothelial cell senescence and vasculopathy in obesity-induced diabetes by ebselen. *Circ Res.* 2004;94:377–384.
32. Losordo DW, Dimmeler S. Therapeutic angiogenesis and vasculogenesis for ischemic disease. Part I: angiogenic cytokines. *Circulation.* 2004;109:2487–2491.
33. Losordo DW, Dimmeler S. Therapeutic angiogenesis and vasculogenesis for ischemic disease. Part II: cell-based therapies. *Circulation.* 2004;109:2692–2697.

Journal of Molecular and Cellular Cardiology 48 (2010) 302–309

Contents lists available at ScienceDirect

Journal of Molecular and Cellular Cardiology

journal homepage: www.elsevier.com/locate/yjmcc

Original article

Activation of MTK1/MEKK4 induces cardiomyocyte death and heart failure

Isamu Mizote [a], Osamu Yamaguchi [a], Shungo Hikoso [a], Toshihiro Takeda [a], Manabu Taneike [a], Takafumi Oka [a], Takahito Tamai [a], Jota Oyabu [a], Yasushi Matsumura [b], Kazuhiko Nishida [a], Issei Komuro [a], Masatsugu Hori [a], Kinya Otsu [a,*]

[a] Department of Cardiovascular Medicine, Osaka University Graduate School of Medicine, 2-2 Yamadaoka, Suita, Osaka 565-0871, Japan
[b] Department of Medical Information Science (Y.M.), Osaka University Graduate School of Medicine, Osaka, Japan

ARTICLE INFO

Article history:
Received 18 July 2009
Received in revised form 20 September 2009
Accepted 9 October 2009
Available online 20 October 2009

Keywords:
MTK1
Heart failure
Apoptosis
p38
JNK

ABSTRACT

MTK1 (MEKK4) is a mitogen-activated protein kinase kinase kinase that regulates the activity of its downstream mitogen-activated kinases, p38, and c-Jun N-terminal kinase (JNK). However, the physiological function of MTK1 in the heart remains to be determined. Here, we attempted to elucidate the function of MTK1 in the heart using *in vitro* and *in vivo* models. MTK1 was activated in the hearts of mice subjected to pressure overload-induced heart failure. Overexpression of a constitutively active mutant of MTK1 (MTK1ΔN) induced apoptosis in isolated neonatal rat cardiomyocytes, whereas a kinase domain-deleted form of MTK1 attenuated H_2O_2-induced apoptosis. Specific inhibitors of p38 or JNK effectively protected cardiomyocytes from MTK1ΔN-induced cell death. In mice, cardiac-specific overexpression of MTK1ΔN resulted in early mortality compared with the lifespan of littermate controls. Echocardiographic analysis revealed increases in end-diastolic and end-systolic left ventricular internal dimensions and a decrease in fractional shortening in MTK1ΔN transgenic mice. In addition, the mice showed characteristic phenotypes of heart failure such as an increase in lung weight. The number of TUNEL-positive myocytes and the level of cleaved caspase 3 protein were both increased in MTK1ΔN transgenic mice. Thus, MTK1 plays an important role in the regulation of cell death and is also involved in the pathogenesis of heart failure.

1. Introduction

In response to mechanical loading or increased systolic wall stress, neurohumoral factors and cytokines are released from the myocardium, resulting in left ventricular dilation and impaired ventricular function. Binding of neurohumoral factors and cytokines to their receptors signals to mitogen-activated protein (MAP) kinase (MAPK) enzyme complex [1]. MAPK plays an important role in cardiac remodeling [2–4]. In mammalian cells, there are at least four subfamilies of MAPKs, namely extracellular signal-regulated kinase (ERK), p38, c-Jun N-terminal kinase (JNK), and ERK5 [5]. Each MAPK is activated via signal cascades that involve MAP kinase kinase kinase (MAPKKK or MEKK) and MAP kinase kinase (MAPKK, MKK or MEK) [5]. The MAPKKKs of the Raf and Mos families activate MEK1/2, whereas other MAPKKKs such as MEKK1/2/3, MAP three kinase 1 (MTK1 or MEKK4), apoptosis signal-regulating kinase 1 (ASK1 or MAPKKK5), transforming growth factor β-activated kinase 1 (TAK1), thousand and one amino acid (TAO) kinases, and mixed lineage kinase (MLK) preferentially activate some or all of MKK3, 4, 6, and 7. MAPKKKs, which are the highest signaling modules, sense the degree of stress-induced cell damage in the upstream phase of the intracellular signaling pathway and determine cell fate by regulation of the MAPK cascade. We and others have previously reported on the roles of the MAPKKKs, such as Raf-1 [6], ASK1 [7], TAK1 [8], and MLK7 [9] in the pathogenesis of cardiac remodeling. Reportedly, Raf-1, ASK1, and TAK1 are associated with cardiomyocyte death and heart failure.

MTK1, also known as MEKK4, is a MAPKKK that regulates p38 and JNK through the phosphorylation of MKK3/6 and MKK4/7, respectively [10,11]. MTK1 is a 182-kDa protein with a single C-terminal catalytic domain and an N-terminal autoinhibitory domain and multiple interaction domains that bind activator proteins such as GADD45-like proteins (GADD45α, β, and γ), Rac, Cdc42, Ccd1, TRAF4, and axin or an inhibitor protein, GSK3β [10,12–14]. Either the phosphorylation of MTK1 by upstream kinases, such as Pyk2, or the binding of an activator protein relieves the autoinhibition and activates downstream signaling pathways [15]. However, the physiological roles of MTK1 remain to be elucidated. In T cells isolated from *MTK1*$^{-/-}$, interferon-γ production is impaired [16], suggesting a role for MTK1 in cytokine production. *MTK1*$^{-/-}$ mice and a dominant negative mutant of MTK1 (*MTK1K/R*) knock-in mice showed defective neural tube development [17,18], suggesting that MTK1 function is critical for neural tube closure. In this study, we attempted to determine the role of MTK1 in the pathogenesis of heart failure. We found that MTK1 is activated in failing hearts and

* Corresponding author.
E-mail address: kotsu@medone.med.osaka-u.ac.jp (K. Otsu).

0022-2828/$ – see front matter © 2009 Elsevier Ltd. All rights reserved.
doi:10.1016/j.yjmcc.2009.10.010

that activation of MTK1 leads to cardiomyocyte death and heart failure.

2. Materials and methods

This study was carried out under the supervision of the Animal Research Committee in accordance with the Guidelines on Animal Experiments of Osaka University and the Japanese Government Animal Protection and Management Law (no. 105).

2.1. Isolation of neonatal rat cardiomyocytes and cell death assay

Ventricular myocytes from 1- to 2-day-old Wister rats were cultured as previously described [19]. Neonatal rat ventricular myocytes were infected for 1 h with adenoviral vectors expressing either wild type MTK1 (Ad-MTK1), a constitutively active mutant of MTK1 (Ad-MTK1ΔN), a kinase domain-deleted form of MTK1 (Ad-MTK1ΔK), a kinase inactive mutant of MTK1 (Ad-MTK1K/R), or β-galactosidase (Ad-LacZ) at a multiplicity of infection of 100 plaque-forming units per cell [10,11]. Three days after infection, cell viability was assessed using the cell titer blue (CTB) assay. The CTB assay, which measures the metabolic activity of viable cells, was carried out using the Cell Titer Blue reagent (Promega) as described previously [20]. Nuclear morphology was observed using 200 μM Hoechst 33258 as described previously [7].

2.2. In vitro kinase assay and Western blot analysis

Thoracic transverse aortic constriction (TAC) was performed on 10-week-old male C57Bl/6J mice as previously described [7]. Neonatal rat cardiomyocytes and mouse hearts were homogenized in a lysis buffer containing 50 mM Tris–Cl, pH 7.4, 150 mM NaCl, 1 mM EDTA, 1 mM EGTA, 2.5 mM Na-orthovanadate, 2.5 mM Na-pyrophosphate, 1 mM Na-β-glycerophosphate, 1% Triton-X 100, and a protease inhibitor cocktail (Roche). Immunoprecipitation of endogenous MTK1 was performed using 300 μg of cardiomyocyte extract or 1000 μg of heart tissue extract and an anti-MTK1 antibody (Sigma). Then, immune complex kinase activity was measured using His-MKK6 as the substrate. Total protein homogenates (20 to 50 μg per lane) were subjected to Western blot analysis using an antibody specific for phospho-p38, phospho-JNK, phospho-ERK1/2, cleaved caspase 3 (Cell Signaling Technology), N-terminus antibody of MTK1 (sc-6846), C-terminus antibody of MTK1 (sc-28770), total p38, total JNK, total ERK1/2, α-tubulin (Santa Cruz Biotechnology), GRP78, GRP94 (Stressgen), caspase12 (Sigma), or GAPDH (Abcam).

Western blots were developed using either the enhanced chemiluminescence (ECL) or ECL-Advance kit (Amersham Pharmacia).

2.3. Histological analyses and evaluation of apoptosis

Heart samples were excised and immediately fixed in buffered 4% paraformaldehyde, embedded in paraffin, and cut into 3-μm thick sections. Hematoxylin and eosin or Azan-Mallory staining was performed on serial sections. Paraffin-embedded heart sections were subjected to the terminal deoxynucleotidyl transferase biotin-dUTP nick end labeling (TUNEL) assay using an *in situ* apoptosis detection kit (Takara). For some samples, triple staining with DAPI, TUNEL, and anti-α-sarcomeric actin antibody (Sigma) was performed.

2.4. Quantitative real-time reverse transcriptase-PCR (QRT-PCR)

Total RNA was isolated from the left ventricle for analysis using the TRIzol reagent (Life Technologies). Levels of atrial natriuretic factor (ANF, *Nppa*) and brain natriuretic peptide (BNP, *Nppb*), and collagen type I (*Col1a2*) mRNA were determined by QRT-PCR, as reported previously [21]. All data were normalized to GAPDH content.

2.5. Generation of MTK1ΔN transgenic mice

Transgenic mice expressing the chloramphenicol acetyltransferase (*CAT*) gene, which was floxed under the CAG promoter, with *MTK1ΔN* downstream, were generated on a C57Bl/6J background. We then crossed the mice with a second transgenic mouse, in which a transgene encoding *Cre* recombinase fused to the mutated estrogen receptor domains was driven by the α-myosin heavy chain promoter (*MerCreMer* mouse) [22]. The 8- to 10-week-old male mice received a single subcutaneous injection of tamoxifen citrate (10 mg/kg body weight) (Sigma) dissolved in 50% ethanol [21]. Echocardiography was performed on conscious mice using ultra-sonography (SONOS-5500, equipped with a 15-MHz linear transducer, Philips Medical Systems) as reported previously [7].

2.6. Statistical analysis

Results are means ± SEM. Paired data were evaluated using the Student's *t*-test and a one-way analysis of variance (ANOVA) with the Bonferroni's post hoc test was used for multiple comparisons. Kaplan–Meier method with Logrank test was used for survival analysis. A value of $P<0.05$ was considered statistically significant.

3. Results

3.1. Activation of MTK1 induces cardiomyocyte death

First, we examined whether MTK1 is activated in failing hearts. Ten-week-old C57Bl/6J mice were subjected to pressure overload by means of TAC. In our model, the mice showed left ventricular dilation and cardiac dysfunction 4 weeks after TAC [7]. We performed an *in vitro* kinase assay to assess MTK1 activity using MKK6 as the substrate. MTK1 activity in pressure-overloaded failing hearts was significantly increased compared with that of sham-operated mouse hearts (Fig. 1A).

To investigate the physiological function of MTK1 in the heart, we constructed adenoviral vectors expressing wild type MTK1 (Ad-MTK1), a constitutively active MTK1 mutant (Ad-MTK1ΔN), a kinase domain-deleted form of MTK1 (Ad-MTK1ΔK), a kinase inactive mutant of MTK1 (Ad-MTK1K/R), and β-galactosidase (Ad-LacZ) (Fig. 1B). Then, we infected neonatal rat cardiomyocytes with adenoviral vectors expressing the MTK1 mutants. Western blot analysis indicates that infection of the adenoviral vectors resulted in the expression of each mutant, but we were not able to detect endogenous MTK1 either in non-infected or viral infected cardiomyocytes (Fig. 1C). Infection with Ad-MTK1ΔN decreased the number of viable cells, as determined using the CTB assay (Fig. 1D). Ad-MTK1 resulted in less cell death compared with Ad-MTK1ΔN. On the other hand, neither Ad-MTK1ΔK nor Ad-MTK1K/R had any effect on cell death. These results indicate that activation of MTK1 results in cardiomyocyte death mediated by MTK1 kinase activity.

To characterize the cell death induced by MTK1 activation, we examined the nuclear morphology of Ad-MTK1ΔN-infected cardiomyocytes by staining with Hoechst dye 33258. The number of cardiomyocytes that showed nuclear fragmentation or chromatin condensation, which are characteristic features of apoptotic cell death, was significantly increased in Ad-MTK1ΔN-infected cardiomyocytes (Fig. 1E, F). Consistent with the morphological analysis, biochemical characterization, determined by Western blot analysis of cleaved caspase 3, revealed that caspase 3 activation was significantly increased in cardiomyocytes infected with Ad-MTK1ΔN (Fig. 1G). Infection with Ad-MTK1 had a similar effect

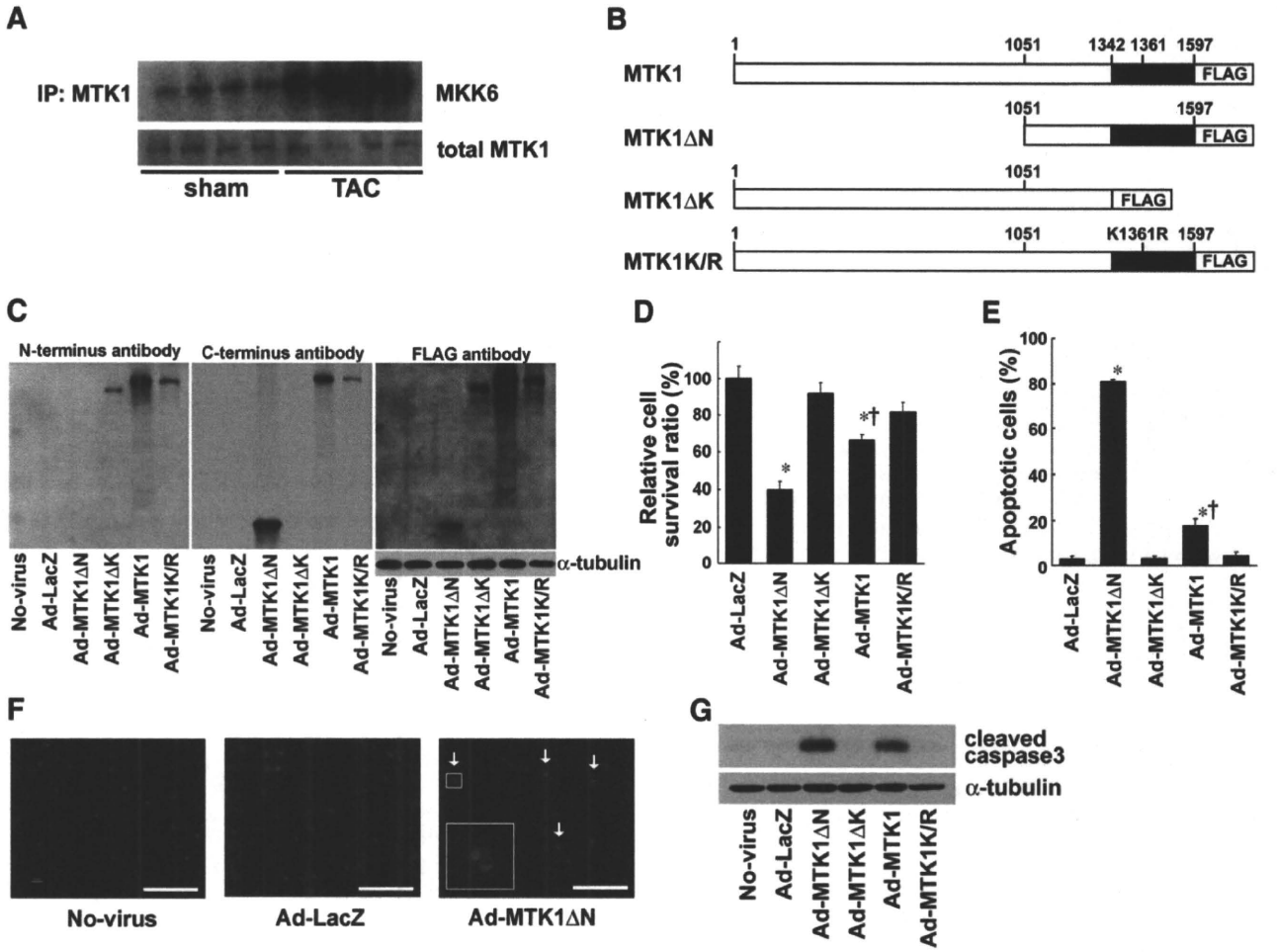

Fig. 1. Activation of MTK1 in failing hearts and its role in apoptosis in isolated cardiomyocytes. (A) MTK1 activity in pressure-overloaded failing hearts. MTK1 activity in sham- or TAC-operated mouse hearts 4 weeks after operation was measured using an immune complex kinase assay with His-MKK6 as the substrate (upper blot). The levels of MTK1 protein are shown in the lower blot. (B) Schematic representation of the mutant MTK1 constructs. The kinase domain of MTK1 is shown as black boxes. MTK1ΔN represents a constitutively active mutant. MTK1ΔK is a kinase domain-deleted mutant. MTK1K/R is a kinase inactive mutant. A FLAG tag was added to the C-terminus of each mutant construct. (C) Western blot analysis of expression of MTK1 mutants and endogenous MTK1 using antibodies against N- and C-termini of MTK1 and FLAG. (D) Cell viability was assessed using the CTB assay. Cell viability was expressed as a ratio relative to the viability of non-infected cardiomyocytes. For the cell viability experiments, neonatal rat cardiomyocytes were infected with each mutant adenovirus at a multiplicity of infection of 100 followed by incubation for 3 days. Values are means ± SEM of 4 independent experiments performed in triplicate. *$P<0.01$ versus Ad-LacZ. †$P<0.01$ versus Ad-MTK1ΔN. (E) Quantification of apoptotic cardiomyocytes 3 days after infection. Apoptotic cells are expressed as a percentage of the total cell number. Values are means ± SEM of 3 independent experiments performed in duplicate. *$P<0.01$ versus Ad-LacZ. †$P<0.01$ versus Ad-MTK1ΔN. (F) Cardiomyocytes were stained with Hoechst dye 33258 three days after infection. White arrows show apoptotic cells with nuclear fragmentation. The larger box is a magnification of the smaller box. (G) Western blot analysis of cleaved caspase 3 in cardiomyocytes 3 days after infection.

on cell death, but the magnitude of the effect was reduced. These results indicate that activation of MTK1 induces apoptotic cell death in cardiomyocytes *in vitro*.

3.2. MAPK signaling is associated with cell death

As reported previously, MTK1 is an upstream activator of MAPKs such as p38 and JNK [10,11]. We examined the level of p38 and JNK activation using Western blot analysis. There were no significant differences in the amount of p38 or JNK protein among cardiomyocytes infected with the mutants (Fig. 2A). However, the amount of phosphorylated p38 and JNK protein was significantly increased in both Ad-MTK1ΔN and Ad-MTK1-infected cardiomyocytes. In addition, the amount of phosphorylated ERK1/2 protein was significantly increased in Ad-MTK1ΔN-infected cardiomyocytes (Fig. 2A), whereas we were not able to detect the phosphorylated ERK5 in any groups (data not shown). To further verify the role of p38 or JNK activation in cardiomyocyte death, we examined the effects of specific inhibitors of p38 (SB203580) or JNK (SP600125) on Ad-MTK1ΔN-induced cell death using the CTB assay. Both SB203580 and SP600125 significantly decreased the number of dead cells and the level of cleaved caspase 3 protein in cardiomyocytes infected with Ad-MTK1ΔN (Fig. 2B–D). Thus, activation of MTK1/p38 and JNK signaling cascades induces cardiomyocyte apoptosis.

3.3. Reactive oxygen species activate MTK1

Reportedly, reactive oxygen species (ROS) are key mediators of apoptosis and heart failure [23]. In the present study, we hypothesized that MTK1 is involved in ROS-induced cell death. To examine this hypothesis, we stimulated cardiomyocytes with H_2O_2 and measured the kinase activity of MTK1. MTK1 was activated by H_2O_2 in a concentration-dependent manner (Fig. 3A). Furthermore, cardiomyocytes infected with Ad-MTK1ΔK were more resistant to H_2O_2, compared with those infected with Ad-LacZ (Fig. 3B). H_2O_2 induced p38 and JNK activation (Fig. 3C, D). Ad-MTK1ΔK inhibited H_2O_2-induced activation of both p38 and JNK. These results indicate

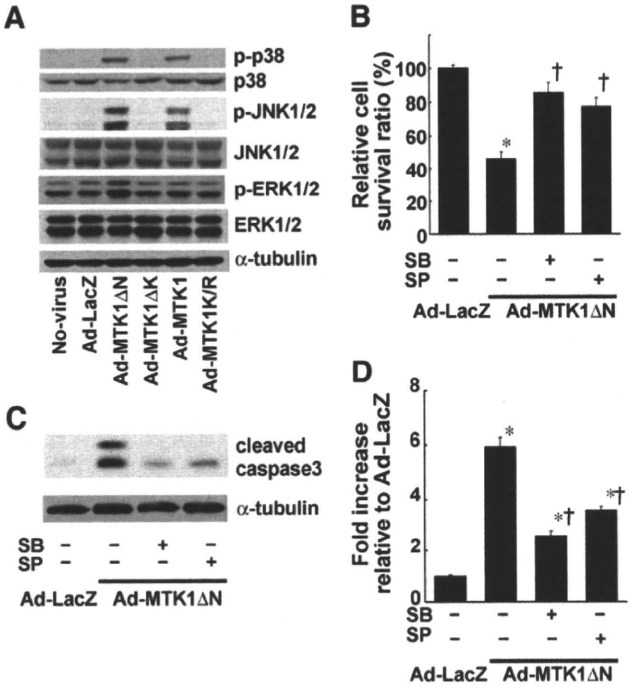

Fig. 2. Assessment of MAPK signaling in cardiomyocytes infected with mutant MTK1. (A) Western blot analysis of phosphorylated (p-) and total p38, JNK1/2, or ERK1/2 three days after infection. (B) Effects of SB203580 (SB) or SP600125 (SP) on MTK1ΔN-induced cell death. Cell viability was assessed using the CTB assay. Cell viability was expressed as a ratio relative to the viability of non-infected cardiomyocytes. Ad-MTK1ΔN-infected cardiomyocytes were incubated for 3 days with or without 20 μM SB203580 or SP600125. Values are means ± SEM of 3 independent experiments performed in triplicate. (C) Western blot analysis of cleaved caspase 3. Isolated cardiomyocytes were infected with Ad-MTK1ΔN and then incubated with or without 20 μM SB203580 (SB) or SP600125 (SP) for 3 days. α-tubulin was used as a loading control. (D) Densitometric analysis of cleaved caspase 3. Data were normalized to α-tubulin content and are expressed as fold increase over that in Ad-LacZ-infected cardiomyocytes. *$P<0.01$ versus Ad-LacZ. †$P<0.01$ versus Ad-MTK1ΔN.

that MTK1 is activated by ROS and that MTK1 activation induces cardiomyocyte death.

3.4. Generation of temporally controlled and cardiac-specific MTK1ΔN transgenic mice

We then examined whether MTK1 activation induces cardiac dysfunction *in vivo*. We generated transgenic mice expressing the floxed *CAT* gene with *MTK1ΔN* downstream (Fig. 4A) and crossed them with other transgenic mice expressing *Cre* recombinase in a tamoxifen-inducible and cardiac-specific manner. In *MTK1ΔN*(+);*Cre*(+) mice treated with tamoxifen, the *CAT* gene should have been floxed out and MTK1ΔN should have been expressed in the heart. MTK1ΔN protein was expressed in the hearts of tamoxifen-treated *MTK1ΔN*(+);*Cre*(+) mice, but not in any other groups treated with (Fig. 4B) or without tamoxifen (data not shown). We were not able to detect endogenous MTK1 in any groups. Tamoxifen treatment resulted in simultaneous activation of p38 and JNK in *MTK1ΔN*(+);*Cre*(+) hearts (Fig. 4C). In addition, ERK1/2 was also activated in tamoxifen-treated MTK1ΔN(+);Cre(+) hearts (Fig. 4C), whereas we were not able to detect the phosphorylated ERK5 in any groups (data not shown). Tamoxifen-treated *MTK1ΔN*(+);*Cre*(+) mice exhibited early mortality compared with *MTK1ΔN*(−);*Cre*(−) mice (Fig. 4D). No *MTK1ΔN*(+);*Cre*(−) or *MTK1ΔN*(−);*Cre*(+) mice treated with or without tamoxifen died during the observation period (data not shown). Another independent transgenic line showed a similar phenotype.

3.5. MTK1ΔN transgenic mice exhibit heart failure

To further investigate the phenotype of the transgenic mouse, we evaluated cardiac function using echocardiography. Before tamoxifen injection, there were no significant differences in

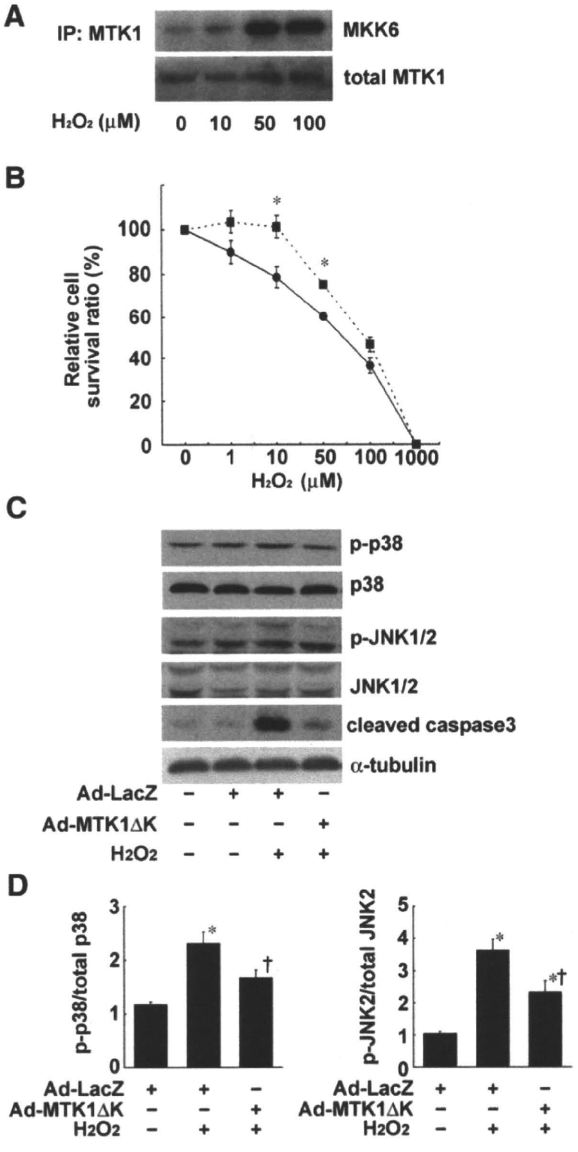

Fig. 3. MTK1 was activated in cardiomyocytes by H_2O_2 stimulation. (A) Neonatal cardiomyocytes were stimulated with H_2O_2 at the indicated concentrations for 3 h. Cell lysates were immunoprecipitated using an anti-MTK1 antibody. MTK1 activity was measured using an immune complex kinase assay with His-MKK6 as the substrate. (B) Neonatal cardiomyocytes were infected with Ad-LacZ or Ad-MTK1ΔK for 3 days and then were stimulated with H_2O_2 for 12 h. Cell viability was assessed using the CTB assay. Cell viability was expressed as a ratio relative to the viability of non-stimulated cardiomyocytes. The circles and squares represent Ad-LacZ- and Ad-MTK1ΔK-infected cardiomyocytes, respectively. Values are means ± SEM of 3 independent experiments performed in triplicate. *$P<0.05$ versus Ad-LacZ at the corresponding H_2O_2 concentration. (C) Neonatal cardiomyocytes were infected with Ad-LacZ or Ad-MTK1ΔK for 3 days and then were stimulated with 50 μM H_2O_2 for 3 h. The cell lysates were subjected to Western blot analysis for phospho- (p-) and total p38 or JNK1/2, and cleaved caspase 3. (D) Densitometric analysis of phosphorylated (p-)/total p38 and JNK2. The density of a sample infected to Ad-LacZ without stimulation was set equal to 1. Values are means ± SEM of 4 independent experiments performed in duplicate. *$P<0.05$ versus Ad-LacZ without H_2O_2 stimulation. †$P<0.05$ versus Ad-LacZ with H_2O_2 stimulation.

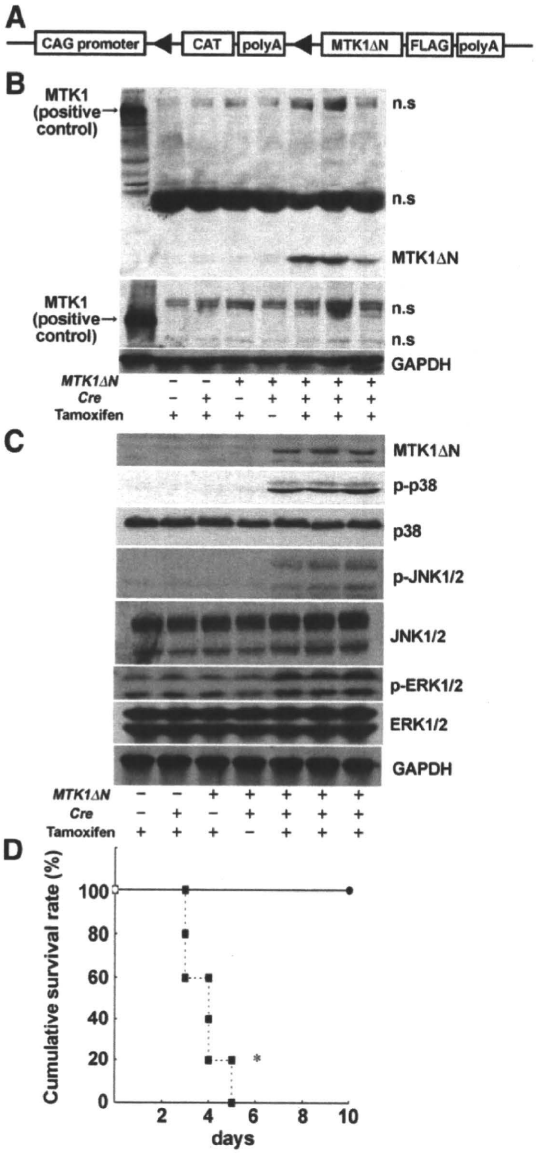

Fig. 4. Generation and characterization of MTK1ΔN transgenic mice. (A) Schematic representation of the construct used for the generation of MTK1ΔN transgenic mice. The *CAT* gene was located between the two lox*P* sites indicated by the arrow heads and was expressed under the CAG promoter. *MTK1ΔN-FLAG* was located downstream from the second lox*P* site. (B) Western blot analysis of expression of MTK1ΔN and endogenous MTK1 using an antibody against C-terminus of MTK1. Upper and lower blot was performed on 7.5% and 5% polyacrylamide gel, respectively. n.s. indicates non-specific band. Overexpressed mouse MTK1 in rat neonatal cardiomyocytes was loaded in the left lane as a positive control. (C) Western blot analysis of expression of MTK1ΔN, phosphorylated (p-), and total p38, JNK1/2, or ERK1/2 two days after tamoxifen treatment. MTK1ΔN was detected using an anti-FLAG antibody. (D) Kaplan–Meier survival analysis of MTK1ΔN transgenic mice. *MTK1ΔN*(+);*Cre*(+) and *MTK1ΔN*(−);*Cre*(−) mice were administered a single subcutaneous injection of tamoxifen. Circles represent *MTK1ΔN*(−);*Cre*(−) mice ($n=10$), squares represent *MTK1ΔN*(+);*Cre*(+) mice ($n=5$). *$P<0.001$ versus *MTK1ΔN*(−);*Cre*(−) mice.

echocardiographic parameters such as diastolic intraventricular septum thickness (IVSd), end-diastolic (LVIDd) and end-systolic (LVIDs) left ventricular internal dimensions, and fractional shortening (FS) among *MTK1ΔN*(−);*Cre*(−), *MTK1ΔN*(−);*Cre*(+), *MTK1ΔN*(+);*Cre*(−) and *MTK1ΔN*(+);*Cre*(+) mice (data not shown). In the control groups, such as *MTK1ΔN*(−);*Cre*(−), *MTK1ΔN*(−);*Cre*(+), and *MTK1ΔN*(+);*Cre*(−), these parameters remained unchanged 2 days after tamoxifen injection (Fig. 5A, B). In *MTK1ΔN*(+);*Cre*(+) mice, IVSd, LVIDd, and LVIDs increased significantly, while FS decreased. Vehicle (ethanol) injection had no effect on the echocardiographic parameters in any groups (data not shown). Before tamoxifen injection, there were no significant differences in physiological parameters, such as heart weight/body weight or lung weight/body weight, among *MTK1ΔN*(−);*Cre*(−), *MTK1ΔN*(−);*Cre*(+), *MTK1ΔN*(+);*Cre*(−), and *MTK1ΔN*(+);*Cre*(+) mice (data not shown). Tamoxifen treatment increased heart weight/body weight, which was used as an index of hypertrophy, in *MTK1ΔN*(+);*Cre*(+) mice (Fig. 5C). Likewise, lung weight/body weight, which was used as an index of lung congestion, also increased in *MTK1ΔN*(+);*Cre*(+) mice. Vehicle injection had no effect on the physiological parameters in any groups (data not shown). Furthermore, we evaluated mRNA levels of *Nppa* and *Nppb*, which are parameters of cardiac remodeling (Fig. 5D). The levels of *Nppa* and *Nppb* mRNA expression were significantly increased only in *MTK1ΔN*(+);*Cre*(+) mice. These results indicate that activation of MTK1 in the heart causes heart failure and early mortality.

3.6. Histological characterization of *MTK1ΔN* transgenic hearts

Consistent with the increased heart weight in tamoxifen-treated *MTK1ΔN*(+);*Cre*(+) mice, hematoxylin-eosin-stained cardiomyocyte sections showed increased cross-sectional areas, compared with tamoxifen-treated *MTK1ΔN*(−);*Cre*(−), *MTK1ΔN*(−);*Cre*(+), or *MTK1ΔN*(+);*Cre*(−) mice (Fig. 6A, B). Azan-Mallory staining demonstrated that interstitial fibrosis was present only in tamoxifen-treated *MTK1ΔN*(+);*Cre*(+) mice (Fig. 6C). The extent of fibrosis was quantified by measuring the level of *Col1a2* mRNA, and it was higher in tamoxifen-treated *MTK1ΔN*(+);*Cre*(+) mice than in the other groups (Fig. 6D). We also assessed the level of apoptosis in the heart using TUNEL staining. There was a significant increase in the number of TUNEL-positive cardiomyocytes in tamoxifen-treated *MTK1ΔN*(+);*Cre*(+) hearts (Fig. 6E, F). TUNEL-positive cells were α-sarcomeric actin-positive, suggesting that the apoptotic cells were cardiomyocytes. Moreover, the level of cleaved caspase 3 protein was significantly increased in the hearts of tamoxifen-treated *MTK1ΔN*(+);*Cre*(+) mice (Fig. 6G).

4. Discussion

The results of the present study show that MTK1 is activated in the heart in a murine model of heart failure induced by pressure overload. MTK1 appears to be involved in cardiomyocyte death, which is believed to a primary cause of heart failure.

MTK1$^{-/-}$ mice or *MTK1K/R* knock-in mice showed enhanced apoptosis in neuroepithelium in the embryo [17,18]. These observations suggest that MTK1 has an anti-apoptotic role. On the other hand, GADD45-like proteins induced apoptosis mediated through MTK1 activation [24]. In the present study, we showed that MTK1ΔN induced apoptosis in neonatal cardiomyocytes, while MTK1ΔK attenuated H_2O_2-induced cardiomyocyte death. MTK1ΔN transgenic mice exhibited heart failure with an increased level of apoptosis. These results suggest a pro-apoptotic role of MTK1. The role of MTK1 might vary with developmental stage or cell-type. Taking into consideration that MTK1 activation was dramatically increased during heart failure induced by pressure overload, MTK1 might be involved in the pathogenesis of heart failure by inducing cell death in response to pressure overload. MTK1ΔK incompletely attenuated H_2O_2-induced cardiomyocyte death with partial inhibition of p38 and JNK, indicating that MTK1 is not the only MAPKKK activated by H_2O_2, which is upstream of p38 and JNK. We previously reported that ASK1, an ROS-dependent MAPKKK, is involved in H_2O_2-induced cardiomyocyte death and the development of heart failure induced by pressure overload [7]. Thus, ROS simultaneously activates various MAPKKKs, such as MTK1 and ASK1,

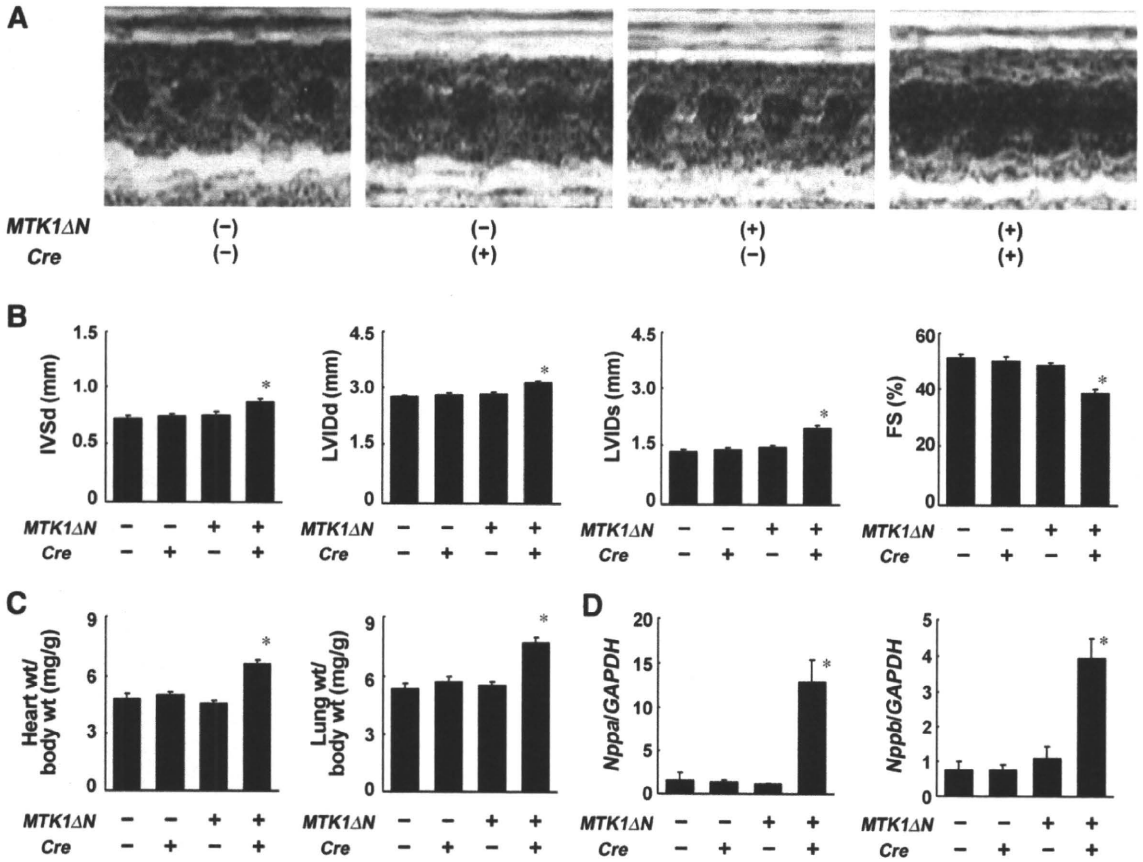

Fig. 5. MTK1ΔN transgenic mice showed heart failure. (A) M-mode echocardiographic tracings from mice 2 days after tamoxifen treatment. (B) Echocardiographic parameters. IVSd, intraventricular septum thickness; LVIDd, end-diastolic left ventricular internal dimension; LVIDs, end-systolic left ventricular internal dimension; FS, fractional shortening. *MTK1ΔN*(−);*Cre*(−) ($n=5$), *MTK1ΔN*(−);*Cre*(+) ($n=8$), *MTK1ΔN*(+);*Cre*(−) ($n=8$), and *MTK1ΔN*(+);*Cre*(+) ($n=10$) mice were treated with tamoxifen. *$P<0.01$ versus all other groups. (C) Heart weight/body weight (heart wt/body wt) and lung weight/body weight (lung wt/body wt) ratios. Tamoxifen-treated *MTK1ΔN*(−);*Cre*(−) ($n=5$), *MTK1ΔN*(+);*Cre*(−) ($n=8$), *MTK1ΔN*(+);*Cre*(−) ($n=8$), and *MTK1ΔN*(+);*Cre*(+) ($n=10$) were analyzed 2 days after treatment. *$P<0.01$ versus all other groups. (D) QRT-PCR analysis of ANF (*Nppa*) and BNP (*Nppb*). Total RNA was subjected to QRT-PCR analysis of *Nppa* and *Nppb*. *Nppa* or *Nppb*/GAPDH ratio in a *MTK1ΔN*(−);*Cre*(−) mouse was set equal to 1. Tamoxifen-treated *MTK1ΔN*(−);*Cre*(−) ($n=7$), *MTK1ΔN*(−);*Cre*(+) ($n=7$), *MTK1ΔN*(+);*Cre*(−) ($n=6$), and *MTK1ΔN*(+);*Cre*(+) ($n=9$) were analyzed. *$P<0.01$ versus all other groups.

to induce apoptosis in cardiomyocytes. Our study provides substantial evidence that increased MTK1 activity is sufficient to induce cardiomyocyte death and cardiomyopathy. However, it has been reported that cardiac-specific overexpression of a protein led to an increase in ER stress and apoptosis [25]. We did not observe an increase in ER stress or the activation of ER stress-dependent caspase, caspase 12, in *MTK1ΔN*(+);*Cre*(+) hearts (Supplementary Fig. 1D). To confirm that MTK1 plays a causal role in the pathogenesis of heart failure, it is necessary to generate cardiac-specific MTK1-deficient mice and to examine their responses to clinically relevant pathological stimuli such as pressure overload or myocardial infarction.

The number of TUNEL-positive cardiomyocytes in MTK1ΔN-overexpressing hearts was consistent with that observed in patients with late-stage dilated cardiomyopathy [26]. However, the rate of apoptosis observed in the present study appears to be too low to induce heart failure in days [27]. The acute occurrence of apoptosis by robust activation of MTK1 may result in degradation of apoptotic cells for a short time. Another possibility is that the causal role of MTK1 in the pathogenesis of heart failure in MTK1ΔN transgenic mice is not apoptosis, but necrosis or contractile dysfunction induced by MTK1 activation. In addition, the reason for the enhanced hypertrophic responses in MTK1ΔN overexpressing hearts is not clear. Hypertrophy is secondary to increased wall stress in dilated chambers. However, we cannot exclude the possibility that MTK1 may directly activate a signal cascade that results in cardiac hypertrophy.

The downstream MAPK signaling cascade of MTK1 reported in previous studies is inconsistent. Overexpression of MTK1 or MTK1ΔN leads to activation of both MKK3/6-p38 and MKK4/7-JNK signaling pathways in COS-7 [11,28] and Hela [11] cells, but to selective activation of MKK4/JNK pathway in HEK293 cells [10]. MTK1K/R inhibited activation of the p38 pathway induced by environmental stresses, but had no effect on activation of the JNK pathway in COS-7 cells [11]. MKK3/6-p38, but not MKK4/7-JNK, activity was inhibited in embryos expressing MTK1K/R [18]. Anti-CD3 antibody- or IL12/IL18-induced p38 activation was reduced in T cells isolated from *MTK1*$^{-/-}$ on a mixed C57Bl/6J×129/SvE background, while activation of JNK was unaffected [16]. By contrast, MTK1K/R inhibited the JNK activation induced by Cdc42/Rac [10], axin [13], and TRAF4 [14]. *MTK1*$^{-/-}$ mice on a C57Bl/6J background showed a reduction of MKK4 activity in the neuroepithelium [17]. These *in vitro* and *in vivo* studies indicate that MTK1 can activate both the p38 and JNK pathways, but the activation pattern of the downstream signaling pathways is dependent on cell-type, the natures of the stress, and the environmental conditions. In cardiomyocytes, we showed that MTK1 activation leads to activation of both p38 and JNK *in vitro* and *in vivo*. Specific inhibitors of p38 and JNK attenuated MTK1ΔN-induced cardiomyocyte death. There is some concern with

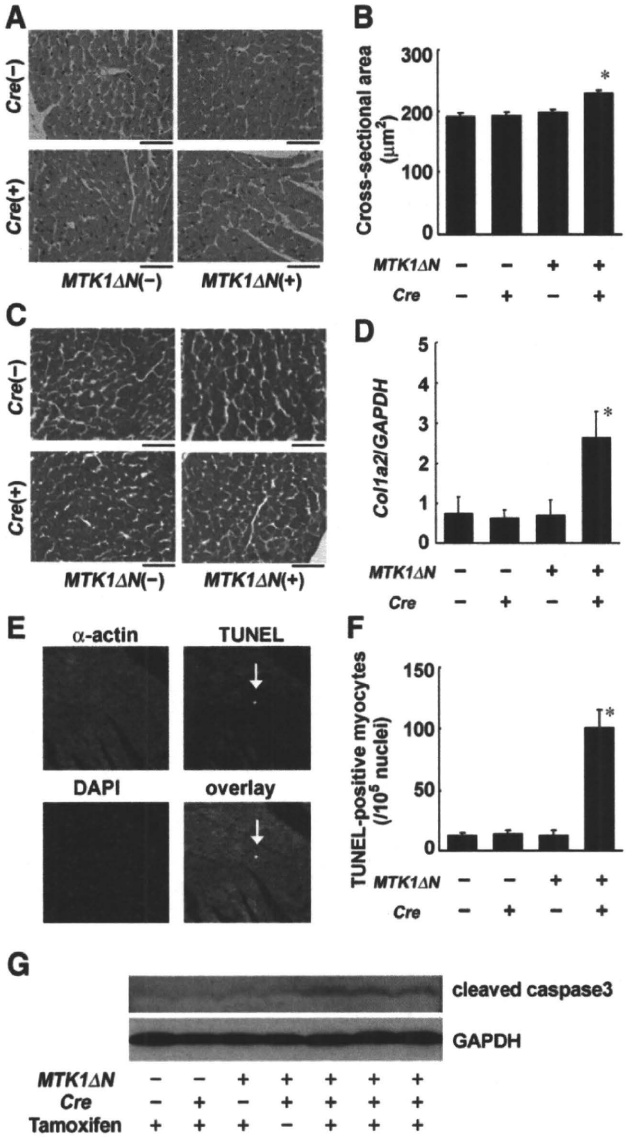

Fig. 6. Histological examination of MTK1ΔN transgenic mice. Histological or biochemical examination was performed 2 days after tamoxifen treatment. (A) Histological analysis of heart sections stained with hematoxylin and eosin. Black bars represent 50 μm. (B) Cardiomyocyte cross-sectional areas. Cross-sectional areas of 100 cells per mouse were measured in random fields. *MTK1ΔN(−);Cre(−)* ($n=5$), *MTK1ΔN(−);Cre(+)* ($n=6$), *MTK1ΔN(+);Cre(−)* ($n=7$) and *MTK1ΔN(+);Cre(+)* ($n=10$). *$P<0.01$ versus all other groups. (C) Histological analysis of heart sections stained with Azan-Mallory. The black bar represents 50 μm. (D) QRT-PCR analysis of collagen type I (*Col12a*). *Col12a*/GAPDH ratio in a *MTK1ΔN(−);Cre(−)* mouse was set equal to 1. *MTK1ΔN(−);Cre(−)* ($n=7$), *MTK1ΔN(−);Cre(+)* ($n=7$), *MTK1ΔN(+);Cre(−)* ($n=6$), and *MTK1ΔN(+);Cre(+)* ($n=8$). *$P<0.05$ versus all other groups. (E) Representative confocal image of TUNEL-positive cardiomyocyte. Triple staining (DAPI, TUNEL, and anti-α-sarcomeric actin antibody) was performed. DAPI-staining is shown in blue. TUNEL-staining is shown in green, and that of α-sarcomeric actin is shown in red. White arrow indicates a TUNEL-positive cardiomyocyte. (F) Number of TUNEL-positive cells. *MTK1ΔN(−);Cre(−)* ($n=3$), *MTK1ΔN(−);Cre(+)* ($n=3$), *MTK1ΔN(+);Cre(−)* ($n=3$), and *MTK1ΔN(+);Cre(+)* ($n=5$). *$P<0.01$ versus all other groups. (G) Western blot analysis of cleaved caspase 3 two days after tamoxifen treatment.

substrate specificity of protein kinase inhibitors, especially SP600125, used in this study [29]. SP600125 has an inhibitory effect on other protein kinases such as SGK, S6K1, AMPK, CDK2, CK1, and DYRK1A. Another JNK inhibitor, JNK inhibitor VIII, has been shown to have no effect on the activity of these kinases [30]. We observed similar effects of JNK inhibitor VIII with SP600125 on MTK1ΔN-induced cardiomyocyte death (Supplementary Fig. 1A–C). Thus, the pro-apoptotic function of MTK1 occurs through both p38 and JNK. We detected activation of ERK1/2 in MTK1ΔN-overexpressed cardiomyocytes or hearts. Taking into consideration that ERK1/2 has a cardioprotective role [31], the ERK1/2 activation will be secondary to MTK1ΔN-induced events towards cell death. It is possible that the ERK1/2 activation may influence on MTK1ΔN-induced cell death and cardiomyopathy.

The p38 and JNK pathways are activated by various stresses [32]. MTK1 is involved in p38 activation induced by various stimuli in a variety of cell types; serum- or heat shock in mouse embryonic fibroblasts [18], anti-CD3 antibody or IL12/IL18 in T cells [16], and osmotic shock, UV irradiation, or anisomycin in COS-7 cells [11]. The results of the present study indicate that MTK1 is activated by pressure overload in mouse hearts and by oxidative stress in isolated cardiomyocytes. Previously, we found that neurohumoral factors (angiotensin II, endothelin I, and phenylephrine) and cytokines (TNF-α) generate ROS in cardiomyocytes *in vitro* [19,33]. In addition, we previously observed an increase in oxidative stress in pressure-overloaded mouse hearts [34]. Thus, it is possible that ROS activate MTK1 during remodeling of the heart. The molecular mechanisms by which ROS activate MTK1 are yet to be elucidated. The role of GADD45-like proteins in the regulation of MTK1 has been studied extensively [12,16,24,35]. GADD45 mRNA is rapidly induced by agents that cause DNA damage (UV and H_2O_2) or by environmental stress [24]. GADD45-like proteins bind and activate MTK1. In the present study, mRNA of GADD45-like proteins was induced in response to H_2O_2, and, in turn, GADD45-like proteins induced cell death in isolated cardiomyocytes (data not shown). These data indicate that GADD45-like proteins might be a candidate activator of MTK1 during cardiomyocyte death. However, the fact that MTK1K/R had no effect on GADD45-like-protein-induced cardiomyocyte death excludes this possibility (data not shown). We previously demonstrated that neurohumoral factors induced activation of Pyk2 and Rac in isolated cardiomyocytes [36,37]. Thus, these signaling molecules might mediate MTK1 activation in cardiomyocytes. Further studies are necessary to elucidate the molecular mechanism underlying MTK1 activation during cardiac remodeling.

In conclusion, we determined that MTK1 is a signaling molecule that induces cardiomyocyte death, cardiac remodeling, and heart failure. Thus, MTK1 might be a therapeutic target for the treatment of patients with heart failure.

Acknowledgments

We thank Jeffrey Molkentin, University of Cincinnati, for the generous gift of the *MerCreMer* mice. This work was supported by a Grant-in-Aid for Scientific Research from the Ministry of Education, Culture, Sports, Science, and Technology, Japan and by Mitsubishi Foundation to K. Otsu.

Appendix A. Supplementary data

Supplementary data associated with this article can be found, in the online version, at doi:10.1016/j.yjmcc.2009.10.010.

References

[1] Opie LH, Commerford PJ, Gersh BJ, Pfeffer MA. Controversies in ventricular remodelling. Lancet 2006;367:356–67.
[2] Liang Q, Molkentin JD. Redefining the roles of p38 and JNK signaling in cardiac hypertrophy: dichotomy between cultured myocytes and animal models. J Mol Cell Cardiol 2003;35:1385–94.

[3] Petrich BG, Wang Y. Stress-activated MAP kinases in cardiac remodeling and heart failure: New insights from transgenic studies. Trends Cardiovasc Med 2004;14: 50–5.
[4] Nishida K, Otsu K. The role of apoptosis signal-regulating kinase 1 in cardiomyocyte apoptosis. Antioxid Redox Signal 2006;8:1729–36.
[5] Kyriakis JM, Avruch J. Mammalian mitogen-activated protein kinase signal transduction pathways activated by stress and inflammation. Physiol Rev 2001;81:807–69.
[6] Yamaguchi O, Watanabe T, Nishida K, Kashiwase K, Higuchi Y, Takeda T, et al. Cardiac-specific disruption of the c-raf-1 gene induces cardiac dysfunction and apoptosis. J Clin Invest 2004;114:937–43.
[7] Yamaguchi O, Higuchi Y, Hirotani S, Kashiwase K, Nakayama H, Hikoso S, et al. Targeted deletion of apoptosis signal-regulating kinase 1 attenuates left ventricular remodeling. Proc Natl Acad Sci USA 2003;100:15883–8.
[8] Zhang D, Gaussin V, Taffet GE, Belaguli NS, Yamada M, Schwartz RJ, et al. TAK1 is activated in the myocardium after pressure overload and is sufficient to provoke heart failure in transgenic mice. Nat Med 2000;6:556–63.
[9] Christe M, Jin N, Wang X, Gould KE, Iversen PW, Yu X, et al. Transgenic mice with cardiac-specific over-expression of MLK7 have increased mortality when exposed to chronic β-adrenergic stimulation. J Mol Cell Cardiol 2004;37:705–15.
[10] Gerwins P, Blank JL, Johnson GL. Cloning of a novel mitogen-activated protein kinase kinase kinase, MEKK4, that selectively regulates the c-Jun amino terminal kinase pathway. J Biol Chem 1997;272:8288–95.
[11] Takekawa M, Posas F, Saito HA. human homolog of the yeast Ssk2/Ssk22 MAP kinase kinase kinases, MTK1, mediates stress-induced activation of the p38 and JNK pathways. EMBO J 1997;16:4973–82.
[12] Mita H, Tsutsui J, Takekawa M, Witten EA, Saito H. Regulation of MTK1/MEKK4 kinase activity by its N-terminal autoinhibitory domain and GADD45 binding. Mol Cell Biol 2002;22:4544–55.
[13] Luo W, Ng WW, Jin L-H, Ye Z, Han J, Lin S-C. Axin utilizes distinct regions for competitive MEKK1 and MEKK4 binding and JNK activation. J Biol Chem 2003;278:37451–8.
[14] Abell AN, Johnson GL. MEKK4 is an effector of the embryonic TRAF4 for JNK activation. J Biol Chem 2005;280:35793–6.
[15] Halfter UM, Derbyshire ZE, Vaillancourt RR. Interferon-γ-dependent tyrosine phosphorylation of MEKK4 via Pyk2 is regulated by annexin II and SHP2 in keratinocytes. Biochem J 2005;388:17–28.
[16] Chi H, Lu B, Takekawa M, Davis RJ, Flavell RA. GADD45β/GADD45γ and MEKK4 comprise a genetic pathway mediating STAT4-independent IFNγ production in T cells. EMBO J 2004;23:1576–86.
[17] Chi H, Sarkisian MR, Rakic P, Flavell RA. Loss of mitogen-activated protein kinase kinase kinase 4 (MEKK4) results in enhanced apoptosis and defective neural tube development. Proc Natl Acad Sci USA 2005;102:3846–51.
[18] Abell AN, Rivera-Perez JA, Cuevas BD, Uhlik MT, Sather S, Johnson NL, et al. Ablation of MEKK4 kinase activity causes neurulation and skeletal patterning defects in the mouse embryo. Mol Cell Biol 2005;25:8948–59.
[19] Hirotani S, Otsu K, Nishida K, Higuchi Y, Morita T, Nakayama H, et al. Involvement of nuclear factor-κB and apoptosis signal-regulating kinase 1 in G-protein-coupled receptor agonist-induced cardiomyocyte hypertrophy. Circulation 2002;105: 509–15.
[20] Nakagawa T, Shimizu S, Watanabe T, Yamaguchi O, Otsu K, Yamagata H, et al. Cyclophilin D-dependent mitochondrial permeability transition regulates some necrotic but not apoptotic cell death. Nature 2005;434:652–8.
[21] Nakai A, Yamaguchi O, Takeda T, Higuchi Y, Hikoso S, Taniike M, et al. The role of autophagy in cardiomyocytes in the basal state and in response to hemodynamic stress. Nat Med 2007;13:619–24.
[22] Sohal DS, Nghiem M, Crackower MA, Witt SA, Kimball TR, Tymitz KM, et al. Temporally regulated and tissue-specific gene manipulations in the adult and embryonic heart using a tamoxifen-inducible Cre protein. Circ Res 2001;89:20–5.
[23] Giordano FJ. Oxygen, oxidative stress, hypoxia, and heart failure. J Clin Invest 2005;115:500–8.
[24] Takekawa M, Saito H. A family of stress-inducible GADD45-like proteins mediate activation of the stress-responsive MTK1/MEKK4 MAPKKK. Cell 1998;95:521–30.
[25] Cook AR, Bardswell SC, Pretheshan S, Dighe K, Kanaganayagam GS, Jabr RI, et al. Paradoxical resistance to myocardial ischemia and age-related cardiomyopathy in NHE1 transgenic mice: a role for ER stress? J Mol Cell Cardiol 2009;46:225–33.
[26] Olivetti G, Abbi R, Quaini F, Kajstura J, Cheng W, Nitahara JA, et al. Apoptosis in the failing human heart. N Engl J Med 1997;336:1131–41.
[27] Wencker D, Chandra M, Nguyen K, Miao W, Garantziotis S, Factor SM, et al. A mechanistic role for cardiac myocyte apoptosis in heart failure. J Clin Invest 2003;111:1497–504.
[28] Abell AN, Granger DA, Johnson GL. MEKK4 stimulation of p38 and JNK activity is negatively regulated by GSK3β. J Biol Chem 2007;282:30476–84.
[29] Bain J, McLauchlan H, Elliott M, Cohen P. The specificities of protein kinase inhibitors: an update. Biochem J 2003;371:199–204.
[30] Szczepankiewicz BG, Kosogof C, Nelson LT, Liu G, Liu B, Zhao H, et al. Aminopyridine-based c-Jun N-terminal kinase inhibitors with cellular activity and minimal cross-kinase activity. J Med Chem 2006;49:3563–80.
[31] Baines CP, Molkentin JD. STRESS signaling pathways that modulate cardiac myocyte apoptosis. J Mol Cell Cardiol 2005;38:47–62.
[32] Karin M. Mitogen-activated protein kinase cascades as regulators of stress responses. Ann N Y Acad Sci 1998;851:139–46.
[33] Higuchi Y, Otsu K, Nishida K, Hirotani S, Nakayama H, Yamaguchi O, et al. Involvement of reactive oxygen species-mediated NF-κB activation in TNF-α-induced cardiomyocyte hypertrophy. J Mol Cell Cardiol 2002;34:233–40.
[34] Date M, Morita T, Yamashita N, Nishida K, Yamaguchi O, Higuchi Y, et al. The antioxidant *N*-2-mercaptopropionyl glycine attenuates left ventricular hypertrophy in in vivo murine pressure-overload model. J Am Coll Cardiol 2002;39: 907–12.
[35] Wang X, Gorospe M, Holbrook NJ. gadd45 is not required for activation of c-Jun N-terminal kinase or p38 during acute stress. J Biol Chem 1999;274:29599–602.
[36] Higuchi Y, Otsu K, Nishida K, Hirotani S, Nakayama H, Yamaguchi O, et al. The small GTP-binding protein Rac1 induces cardiac myocyte hypertrophy through the activation of apoptosis signal-regulating kinase 1 and NF-κB. J Biol Chem 2003;278:20770–7.
[37] Hirotani S, Higuchi Y, Nishida K, Nakayama H, Yamaguchi O, Hikoso S, et al. Ca^{2+}-sensitive tyrosine kinase Pyk2/CAKβ-dependent signaling is essential for G-protein-coupled receptor agonist-induced hypertrophy. J Mol Cell Cardiol 2004;36:799–807.

Research article

Excessive cardiac insulin signaling exacerbates systolic dysfunction induced by pressure overload in rodents

Ippei Shimizu,[1] Tohru Minamino,[1,2] Haruhiro Toko,[1] Sho Okada,[1] Hiroyuki Ikeda,[1] Noritaka Yasuda,[1] Kaoru Tateno,[1] Junji Moriya,[1] Masataka Yokoyama,[1] Aika Nojima,[1] Gou Young Koh,[3] Hiroshi Akazawa,[1] Ichiro Shiojima,[4] C. Ronald Kahn,[5] E. Dale Abel,[6] and Issei Komuro[1,4]

[1]Department of Cardiovascular Science and Medicine, Chiba University Graduate School of Medicine, Chiba, Japan. [2]PRESTO, Japan Science and Technology Agency, Saitama, Japan. [3]Biomedical Research Center and Biological Sciences, Korea Advanced Institute of Science and Technology, Daejeon, Korea. [4]Department of Cardiovascular Medicine, Osaka University School of Medicine, Osaka, Japan. [5]Joslin Diabetes Center, Harvard Medical School, Boston, Massachusetts, USA. [6]Division of Endocrinology, Metabolism and Diabetes and Program in Molecular Medicine, University of Utah School of Medicine, Salt Lake City, Utah, USA.

Although many animal studies indicate insulin has cardioprotective effects, clinical studies suggest a link between insulin resistance (hyperinsulinemia) and heart failure (HF). Here we have demonstrated that excessive cardiac insulin signaling exacerbates systolic dysfunction induced by pressure overload in rodents. Chronic pressure overload induced hepatic insulin resistance and plasma insulin level elevation. In contrast, cardiac insulin signaling was upregulated by chronic pressure overload because of mechanical stretch–induced activation of cardiomyocyte insulin receptors and upregulation of insulin receptor and Irs1 expression. Chronic pressure overload increased the mismatch between cardiomyocyte size and vascularity, thereby inducing myocardial hypoxia and cardiomyocyte death. Inhibition of hyperinsulinemia substantially improved pressure overload–induced cardiac dysfunction, improving myocardial hypoxia and decreasing cardiomyocyte death. Likewise, the cardiomyocyte-specific reduction of insulin receptor expression prevented cardiac ischemia and hypertrophy and attenuated systolic dysfunction due to pressure overload. Conversely, treatment of type 1 diabetic mice with insulin improved hyperglycemia during pressure overload, but increased myocardial ischemia and cardiomyocyte death, thereby inducing HF. Promoting angiogenesis restored the cardiac dysfunction induced by insulin treatment. We therefore suggest that the use of insulin to control hyperglycemia could be harmful in the setting of pressure overload and that modulation of insulin signaling is crucial for the treatment of HF.

Introduction

Cardiac hypertrophy is defined as an increment of ventricular mass resulting from increased cardiomyocyte size and is the adaptive response of the heart to an increased hemodynamic load due to either physiological factors such as exercise or pathological states such as hypertension and valvular diseases (1). Exercise-induced cardiac hypertrophy does not progress to heart failure (HF) (2, 3) and therefore is thought to be "physiological hypertrophy." On the other hand, pressure overload initially induces "adaptive hypertrophy," but causes "maladaptive (pathological) hypertrophy" in the chronic phase that results in HF (1).

Several signaling pathways have been implicated in the development of physiological or pathological cardiac hypertrophy. The insulin/PI3K/Akt axis plays a crucial role in the development of physiological hypertrophy as well as in normal cardiac growth, whereas activation of G-protein–coupled receptors in collaboration with PKC and calcineurin/nuclear factor of activated T cells (NFAT) pathways is involved in the development of pathological hypertrophy (4). Although homozygous cardiomyocyte-specific insulin receptor knockout (CIRKO) mice have smaller hearts than WT controls (5), both WT and CIRKO mice have shown a comparable increase of cardiac mass in response to pathological hypertrophic stimuli such as pressure overload (6). Overexpression of constitutively active p110α, a catalytic component of PI3K, in the heart has led to enhanced cardiac growth with preserved systolic function (7). Conversely, myocardial expression of dominant-negative p110α has inhibited the physiological hypertrophic response during postnatal growth and following exercise in mice, whereas the response to pressure overload has not been altered (8). Likewise, homozygous *Akt1*-deficient mice have shown defective exercise-induced cardiac hypertrophy (9), further supporting a crucial role of the insulin/PI3K/Akt pathway in physiological hypertrophy and growth of the heart.

Besides their role in physiological hypertrophy and normal cardiac growth, insulin signals may induce pathological hypertrophic responses. It has been shown that chronic hyperinsulinemia stimulates angiotensin II signaling that is involved in pathological hypertrophy (10). Mild to moderate activation of Akt was shown to induce cardiac hypertrophy with preservation of function (11, 12), whereas high levels of activated Akt expression in the heart led to pathological hypertrophy (13). Short-term Akt activation induced physiological cardiac hypertrophy, but constitutive activation of this pathway led to cardiac dysfunction (14). In this state, coordinated tissue growth and angiogenesis in the heart were disrupted, leading to myocardial hypoxia (14). Likewise, it has been demonstrated that chronic pressure overload increases the mismatch between cardiomyocyte size and vascularity and therefore induces

Authorship note: Ippei Shimizu and Tohru Minamino contributed equally to this work.

Conflict of interest: The authors have declared that no conflict of interest exists.

Citation for this article: *J Clin Invest.* 2010;120(5):1506–1514. doi:10.1172/JCI40096.